# MULTIPHASE EQUILIBRIUM OF FLUIDS CONFINED IN FISCHER-TROPSCH CATALYTIC SYSTEMS

A Thesis

by

SAMAH ESSAM-ELDIN WARRAG

Submitted to the Office of Graduate and Professional Studies of
Texas A&M University
in partial fulfillment of the requirements for the degree of

MASTER OF SCIENCE

| | |
|---|---|
| Chair of Committee, | Nimir Elbashir |
| Co-Chair of Committee, | Marcelo Castier |
| Committee Member, | Khalid Qaraqe |
| Head of Department, | M. Nazmul Karim |

May 2014

Major Subject: Chemical Engineering

**ABSTRACT**

Energy supply and security imposes a significant challenge in our modern world stemming from our dependence on depleting resources such as petroleum and oil. Fischer-Tropsch synthesis (FTS) is considered as a great energy alternative which can significantly reduce our dependence on oil, improve rural economics, reduce greenhouse emissions, and promise energy security. It is a key technology for converting syngas, produced from coal, biomass or natural gas, into a variety of hydrocarbon products. Although this technology was discovered in 1923, commercialization and scale up are limited to the use of few reactor configurations (e.g. multi-tubular fixed-bed reactor, Slurry-bubble column reactor, and fluidized bed reactors).

In order to improve the limitations in both reactor configurations, on lab scale near critical media was utilized, since it offers a great combination of the advantages of both the gas-phase reaction (multi-tubular fixed-bed reactor) and the liquid-phase reaction (slurry-bubble column reactor), while simultaneously overcoming their limitations. This work focuses on modeling the phase behavior of the FTS mixture in fixed bed reactor in the bulk phase inside the reactor bed or inter-particle and then zoom into the catalyst (confined phases within the catalyst pores or intra-particle). This is done by using an extended Peng-Robinson (PR) equation of state (EOS) that is capable of accounting for the fluid behavior inside confined pores as well as in the bulk phases.

The PR Equation of state model extended to confined fluid (PR-C) has been utilized in multiphase equilibrium algorithm using FORTRAN. The simulation results

provide the composition and the condition of each bulk phase and pore phase for a given initial mixture. Two different scenarios were studied for fixed bed reactor: the first one is the conventional gas phase FTS and the second one is for the supercritical phase FTS (SCF-FTS). In each case, the phase behavior of the mixture of the reactants and products was investigated at different conversions along the bed length. The simultaneous assessment of both gas phase FTS and SCF-FTS phase behavior and reaction performance open the door for optimizing the design FTS reactor and enhance the efficiency of the process.

Preferential adsorption of hydrogen has been observed and this could be due to the small size of the hydrogen molecules compared to those of the other components. Our studies suggested that the supercritical phase provides superior heat dissipation due to the existence of denser phase in the bulk and the confined regions than the conventional gas phase. On the other hand in the gas phase and for limited carbon number (up to $C_8$) the pore phase is found to be in a vapor state which should provide higher diffusivity of the reactant than that in the supercritical phase. Our study will continue by integrating the developed phase behavior studies in the reactor design model

# DEDICATION

I dedicate my dissertation work to my family and friends. A special gratitude to my loving parents, whose words of encouragement and push for tenacity ring in my ears. I also dedicate this dissertation to my many friends who have supported me throughout the process.

# ACKNOWLEDGEMENTS

I would like to thank my committee chair, Dr. Nimir Elbashir, and my committee co-chair, Dr. Marcelo Castier, for their guidance and support throughout the course of this research. Their comments and recommendations to elevate the work quality educated me and helped me to finish this work.

Thanks also go to my friends and colleagues and the department faculty and staff for making my time at Texas A&M University at Qatar a great experience.

Also, I would like to acknowledge the finical support and collaboration in this project by Qatar National Research Fund (NPRP 5-066-2-023) members of Qatar Foundation. The statements made herein are solely the responsibility of the author.

Finally, thanks to my mother and father for their encouragement and to my friends for their love and support.

# NOMENCLATURE

| | |
|---|---|
| $a_p$ | Confinement-modified energy parameter of the equation of state |
| $b_p$ | Confinement-modified volume parameter of the equation of state |
| $A$ | Helmholtz free energy |
| $E_{conf}$ | Configurational energy |
| $F_{pa}$ | Fraction of the confined molecules subject to the pore wall attractive field for random distribution of the molecules inside the pore. |
| $k$ | Boltzmann constant |
| $N$ | Total number of molecules |
| $N_{av}$ | Avogadro's number |
| $P$ | Pressure |
| $q$ | Internal partition function of one molecule |
| $Q$ | Canonical partition function |
| $R$ | Universal gas constant |
| $r_p$ | Pore radius |
| $T$ | Absolute temperature |
| $v$ | Molar volume |
| $V$ | Total volume |
| $V_f$ | Free volume |
| $x$ | Mole fraction |
| $\delta_p$ | Square well width of the molecule-wall interaction potential |
| $\varepsilon_p$ | Square well depth of the molecule-wall interaction potential |
| $\lambda$ | De Broglie wavelength |
| $\rho_{max}$ | Confinement-modified molecular packing density |
| $\sigma$ | Molecular diameter |
| $i, j$ | Indices denote components |
| $NC$ | Index denotes the number of fluid components |

$\alpha$    Chain growth probability

$n$    Index denotes carbon number

# TABLE OF CONTENTS

Page

# LIST OF FIGURES

Page

# LIST OF TABLES

# 1. INTRODUCTION AND LITERATURE REVIEW

## 1.1 Thermodynamics and Equation of States Capabilities

Thermodynamics is the branch of science that relates the properties of a given system to parameters that are readily measured, and thus provides a good knowledge of the system behavior and a maximum return of information for any investment in laboratory experiments. In thermodynamics, relationships are known as equations of state (EOS) are mathematical models between two or more state variables such as temperature, pressure, volume, internal energy or others that describes the state of the system under any given conditions. EOSs are widely used for the calculation of thermodynamic properties, phase behavior, and phase equilibrium of pure components and of mixtures. The knowledge of these properties over a wide range of temperature, pressure and composition is crucial for the design of a broad range of processes in a variety of industrial applications that include oil and gas and specialty chemicals including polymers, pharmaceuticals, and cosmetics and for environmental control.

The first EOS for non-ideal fluids was proposed by Van der Waal in 1873 at his doctorate thesis entitled "**On the Continuity of the Gaseous and Liquid State**"[1]. It was the first thermodynamic model applicable to both gas state and liquid state of fluids. The Van der Waals (vdw) EOS was the origin of a well-known class of equations of state called the **cubic equations of state** such as Peng Robinson (PR) [2], Soave-Redlich-Kwong (SRK) [3], Patel-Teja [4] and others. The latter EOSs are extensions and modifications of the vdw model that cover extended temperature and pressure ranges to include subcritical, near-critical and supercritical conditions. In addition, improved

1

applicability to fluids of variable molecular size from small spherical molecules (e.g., gases) to long-chain molecules (e.g., heavy hydrocarbons and polymers) as well as to fluids whose molecules exhibit non-polar, polar and hydrogen-bonding interactions [5]. The vdw model has also been extended to multicomponent mixtures of components that may be similar or very dissimilar in terms of molecular size, shape and interactions by applying appropriate mixing rules [5].

Due to the simplicity of the mathematical computation and the reasonable accuracy in the prediction of thermodynamic properties and phase equilibrium for both pure components and mixtures, the EOSs dominated the oil and gas industry applications and processes simulators for decades [5]. Over the past century, numerous review papers and book chapters on the cubic and generalized vdw EOS have appeared in the open literature discussing some of the major developments of the cubic EOSs while addressing their mixing rules, and the challenges these EOS face in predicting properties of fluids in near critical and within the supercritical regions [5-9].

The cubic equations of state provide information of the system's thermodynamic behavior of bulk fluids at the macroscopic scale. However, as the size of a system decreases to a microscopic level, the effect of the confinement on the properties of the fluid becomes more pronounced. In this case a combination of surface tension (which is caused by cohesion forces within the fluid) and adhesive forces between the fluid and the confining solid will act on the fluid. Thus, the properties of a fluid confined in small spaces, such as cavities of a porous solid may differ substantially from those observed in the non-confined state (i.e., on a macroscopic scale).

As mentioned above, the differences in the thermodynamic properties of a fluid confined from those of the same, bulk fluid impose a challenge in modeling many technical applications such as adsorption-based separation processes, extraction of oil entrapped in the small cavities of reservoir rocks, and complex adsorption in heterogeneous catalytic systems. Unlike all the complex models adopted to model the adsorption behavior (e.g. molecular simulation[10]), an EOS represents a simple way of calculating these properties and describing the thermodynamic behavior of the confined fluids. An appropriate EOS for this purpose must explicitly represent the effect of the confinement such as the pore size (i.e., size parameter) and intensity of interaction (i.e., energy of interaction parameter) between the molecules of fluid and the pore walls. Also, one of the challenges in modeling adsorption systems is the representation of the structural heterogeneity of the solid adsorbents which can strongly influence the system behavior. Therefore, by developing such equation of state it would be possible to describe the behavior of a fluid confined in pores of different sizes, using the same set of parameters.

A successful attempt has been made by Travalloni et al. [11-13] to develop an EOS that describes the fluid properties in the bulk and confined phases. They extended two of the well-kwon cubic EOSs, which are van dar Waals and Peng-Robinson EOSs starting from the Generalized van der Waals theory [14]. The characteristic pore size and the characteristic energy of interaction between the molecules of the fluid and the confining wall are adjustable parameters of the model which can be quantified by fitting adsorption experimental data [12]. One unique feature of this model is its ability to simultaneously account for the effect of more than one type of pore (i.e. different sizes and interaction

3

energies) which allows the modeling of heterogeneous adsorbents [11, 12]. With this development, the same equation of state can be used to model the fluid confined inside the adsorbent pores and in the bulk phase, which is represented as confined by the walls of infinitely large pore and zero interaction energy in such a way that is the effect of the pore walls on thermodynamic properties is negligible. Moreover, with a model of such characteristics, algorithms currently used in the calculations of macroscopic phase equilibrium could be easily adapted to problems of adsorption equilibrium [11, 12].

This research work will focus on applying the EOS for confined fluids proposed by Travalloni et al. [11-13] on heterogeneous catalytic systems, more specifically the Fisher-Tropsch synthesis (FTS) to carry out multi-equilibrium calculations between the bulk phases and the confined phases inside the catalyst pores. The following sections will give a brief background of the FTS and its relevance to the work of modeling the confined fluids.

**1.2 Research Background**

*1.2.1 Fischer-Tropsch Synthesis (FTS)*

The Fischer–Tropsch synthesis is a catalyzed polymerization reaction that converts synthesis gas or syngas (a mixture of carbon monoxide (CO) and hydrogen ($H_2$)) into gaseous and liquid hydrocarbons mixture of wide range of carbon numbers. This chemistry was discovered by Franz Fischer and Hans Tropsch at the Kaiser Wilhelm Institute for Coal Research (presently, Max Plank Institute) at Mülheim (Ruhr), Germany in 1925 [15].The overall stoichiometry can be described by the following reaction [16]:

$$(2n + 1)H_2 + nCO \rightarrow C_nH_{2n+2} + nH_2O \quad -\Delta H = -167 \ KJ/mol/CO \quad (1.1)$$
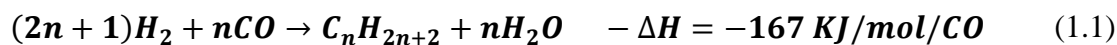
The FTS represents the heart of the X-to-Liquid Technology referred to as XTL (where X = C for coal, = G for natural gas or = B for biomass). In XTL, the feedstock could be coal, natural gas or biomass that needs to be converted first into syngas through gasification (for coal and biomass) or reforming (for natural gas). Syngas will then be fed to the FTS reactor to form liquid hydrocarbons with different chain lengths. Finally, the hydrocarbons products will be upgraded for the production of fuels and chemicals (see Figure 1)
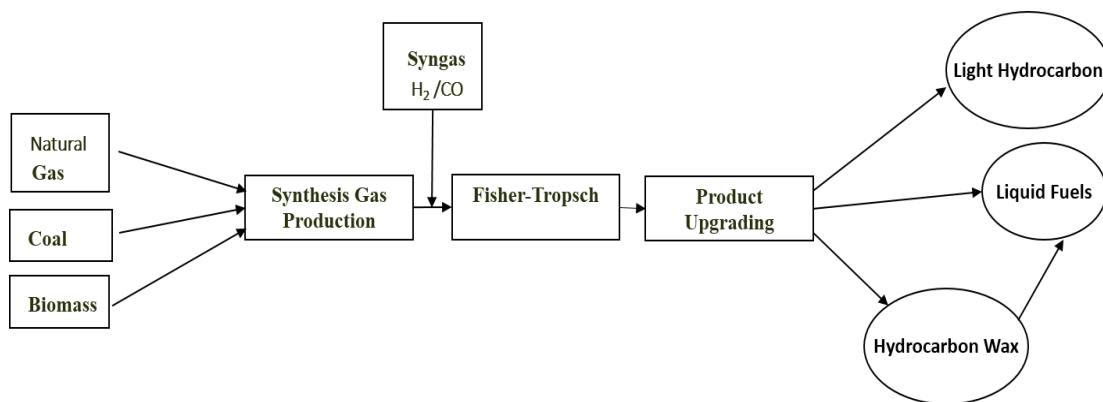


**Figure 1:** Fisher -Tropsch synthesis flow diagram

### 1.2.2 Reactors for Fisher- Tropsch Synthesis

FTS products attract attention as a source of ultra-clean fuels because of their very low-sulfur content and lack of aromatics[15, 17]. Different catalytic systems (mainly cobalt-based catalysts or iron-based catalysts) as well as several types of reactor

technologies have been utilized for FTS. Two of these reactors have become the focus of the recent commercial XTL processes (the multi-tubular fixed-bed reactor, and the slurry reactor) [15].

The State of Qatar has a vast availability of natural gas "Row stock for GTL processes" which is ranked as the third largest natural gas reserves in the world with a total capacity of 910 tcf [18]. This has motivated Qatar to establish several liquefied natural gas (LNG) plants and two world-class commercial-scale GTL plants: Oryx GTL Plant, which is a joint venture between Qatar Petroleum and Sasol and the world largest GTL plant, the Pearl GTL, which belongs to Shell and is based on its technology. For the FTS reactors, Sasol currently utilizes the slurry-bubble column reactor while Shell uses the FTS fixed-bed reactors.

 Slurry reactors operate in three-phase regime (solid/liquid/gas) in which small catalyst particles are suspended within a waxy hydrocarbon solvent. The synthesis gas is bubbled through this medium and, as it passes along the catalyst particles, it reacts to form the products. The lighter compounds evaporate out of the reactor and are collected downstream. The heavier products remain for longer periods of time inside the reactor and become part of the waxy solvent, which is extracted continually as it is formed [15].

The slurry phase is semi homogenous and this enhances many transport properties such as bringing reactants and catalysts together and removing heat from the reactor, which is essential for such highly exothermic reactions like the FTS reactions. In addition, the hydrocarbon solvent acts as a buffer ensuring that the heat generated does not lead to an extreme temperature rise. The improved control of the reactor temperature also leads

to improved control over the product distribution and has significant positive effects on catalyst lifetime. On the other hand, the catalysts experience significant friction, resulting in strict requirements for catalyst strength and difficulties in wax-catalyst separation[15].

In the multi-tubular fixed Bed Reactor a number of narrow tubes are stacked parallel to one another in a single reactor vessel. Each tube is packed with a bed of catalyst pellets. The syngas flows through the catalyst bed in each tube where it reacts at the active sites within the catalyst pellet. In between these tubes, a coolant is used to remove the reaction heat from the tubes and to control the temperature over the bed, which is critical for this case since the gas phase has poor heat capacity compared to heavy hydrocarbon solvent for the slurry reactor. Nevertheless, this type of reactor setup provides high reactant diffusivity and reaction rates. However, as the products form, a large amount of heat is generated leading to local overheating of the catalyst surface 'hot spots', which may affect the catalyst activity. Moreover, the waxy hydrocarbon products of this synthesis cause pore blockage and creates mass transfer and diffusional limitations [15].

*1.2.3 Supercritical Fluids in Fischer-Tropsch Synthesis (SCF-FTS)*

It has been shown that the advantages of efficient gas diffusivity coupled with the greater conversion rate in fixed bed reactors and the dense liquid phase which offers great heat buffering in the slurry reactors can be combined via utilization of supercritical fluids (SCF)[19]. Co-feeding SCFs with the gaseous reactants ($CO+H_2$) can offer certain advantages over traditional FTS reactions including the ability to manipulate the reaction environment through simple changes in pressure. SCF solvents offer attractive transport properties including: low viscosity and high diffusivity, resulting in superior mass transfer characteristics and in-situ extraction to the waxy FTS reaction products within the catalyst pores [19]. Moreover, high compressibility near the critical point induce large changes in density with very small changes in pressure and/or temperature, enabling great heat dissipation and great catalyst maintenance [19, 20].

The proposed SFC-FTS has not been carried out beyond lab scale. More thorough understanding of the transport and thermodynamic behavior of the unique reaction medium would offer great benefits to investigate the scalability via modeling [19, 20].

As outlined earlier, FTS is a multiphase reaction in which syngas is converted in the presence of catalyst, into a mixture of hydrocarbons and water. Complete design and optimization of FTS fixed bed reactors may strongly depend on the presence of a liquid phase creating a boundary layer around the catalyst pellets and blocking their pores. Accordingly, thorough knowledge of the thermodynamics of the reaction mixture and phase characterization (i.e. phase equilibrium calculations) is required.

8

The approach in this research work is to investigate the nature of the phases co-existing in the FTS fixed bed reactors and within its catalyst pores. This will be achieved by applying the EOS model for confined fluids to carry out phase behavior studies in the macro-scale (bulk phase inside the reactor bed or inter-particle) and then zoom in to the micro-scale (confined phases within the catalyst pores or intra-particle).

*1.2.4 Product Synthesis*

It has been shown that FTS is a stepwise polymerization reaction which can be described as follows for a cobalt-based catalyst for example [15]:

1. Reactant (CO) diassociatively adsorbed on the catalyst as well as the $H_2$. The adsorbed C and H molecules then react at the catalyst surface to form methyl species ($CH_3$).

2. Chain growth via sequential addition of $CH_2$ groups and insertion of additional CO molecules followed by hydrogenation.

3. Chain termination which occur at any time during the chain growth process to yield either *α*-olefin or an *n*-paraffin once the product desorbs. Also, other reactions take place such as methanation (to form $CH_4$) and formation of $H_2O$ (significant amount of water produced during FTS as for each one mole CO consumed one mole of water produced) and formation of $CO_2$.

4. Product desorption from the catalyst surface.

The chain polymerization model known as the Anderson-Shulz-Flory (ASF) model is represented by the following equation [21]:

$$x_n = (1 - \alpha)a^{n-1} \tag{1.2}$$

where $x_n$ is the mole fraction of the hydrocarbon with a carbon number $n$ and $\alpha$ is the carbon number independent constant chain growth probability. Classically $\boldsymbol{\alpha}$ is considered as constant value determined experimentally and independent of the carbon number. It has been shown experimentally that the FTS product distribution could deviate from the ideal ASF product distribution [16]. In the current study the chain growth probability has been determined using carbon number dependent definition of the chain growth probability. The approach adopted here is described elsewhere [21].

# 2. RESEARCH PROBLEM AND OBJECTIVES

## 2.1 Research Problem

In the commercial fixed-bed FTS reactor the catalyst particle size is 1 mm. These catalyst particles, either cylindrical or spherical, represents an active site composed of either cobalt or alumina supported on alumina or silica [15, 17]. As described earlier, the synthesis process starts with a ($CO+H_2$) gas mixture "Syngas" fed to the reactor, adsorbed at the catalyst active sites that either exist at the surface of the support or inside the catalyst pores. As the reaction proceed, the following products form: a series of hydrocarbons, water, and $CO_2$ is been produced [15, 17]. As the reaction proceeds heavy hydrocarbons could condense and fill the catalyst pores due to the high capillary pressure. This limits the mass transfer process by restricting the flow of reactants from the bulk phase to the active site and the products from the catalyst pores to the bulk phase and as a result this phenomenon will decrease the accessibility to the active sites. Understanding the phase behavior of such mixture inside the confined pores is quite critical for maximizing the utilization of these active sites. The driving force behind the utilization of the so-called SCF-FTS is thought to provide a single phase for the syngas and the products, and, therefore, minimize the possibility of pore condensation and mass transfer barriers. Limited efforts have been devoted to quantify the influence of utilizing the SCF on the phase behavior either in the bulk fluid (i.e., macro-scale or inter-particle) or inside confined catalyst pores (i.e., micro-scale or intra-particle).

The focus of current research activities in SCF-FTS is to:

- Develop an appropriate EOS capable of predicting the phase behavior of the reaction mixture for the non-ideal near and supercritical phase, specifically inside the catalyst pores (confined phase behavior).

- Understand the role of supercritical solvent and its influence on the inter-particle and intra-particle behavior.

- Develop correlations between the reaction conditions (temperature and pressure) and the thermo-physical characteristics of the reaction mixture.

This research work attempts to model the phase behavior of FTS in fixed bed reactors using an extended Peng-Robinson EOS that is capable of accounting for the fluid behavior inside confined pores as well as in the bulk phases. Two different scenarios will be studied: the first one is conventional gas phase FTS and the second one is for the super-critical phase FTS. In each case, the reactants and products mixture phase's nature will be investigated at different conversions along the bed length. The simultaneous assessment of both the gas phase FTS and SCF-FTS will also aid to compare the performance of the supercritical phase and of the conventional gas phase FTS.

## 2.2 Research Objectives

In this proposed research, the main objective is to characterize the nature of the phases existing in the bulk and confined within the catalyst pores. Another goal is to verify whether or not capillary condensation caused by the reaction mixture at the typical reaction conditions does exit, as claimed by several studies reported in literature[19, 22, 23]. Moreover, an additional target is to check, whether by utilizing supercritical fluids in FTS will provide significant enhancement to the in-situ mass and heat transfer limitation.

The tasks involved in order to achieve the thesis goals specified before were as follows:

1. Conduct an extensive literature review.

2. Understand the thermodynamic model for confined fluids that was used.

3. Collect the experimental data required to use the EOS model and estimate its adjustable parameters.

4. Set up the phase behavior problem for FTS conditions and conduct multi-phase equilibrium calculations for bulk and confining region within the catalyst.

More details on these activities are given in Chapter 3.

# 3. RESEARCH METHODOLOGY

## 3.1 Research Plan

This section of the thesis describes the approach used to complete this research project. The objectives specified previously for this research are related directly to the tasks summarized in Table 1.

**Table 1**: Research plan

| Task | Methodology |
|---|---|
| **Task 1:** Conduct an extensive literature review. | • Conduct an extensive literature review to provide a comprehensive understanding of the research framework, develop a research problem and objectives and identify appropriate methodology to achieve research objectives.<br>• Provide a summary of the main related published research work on the following topics:<br>  ➢ The thermodynamic modeling of confined fluids in homogenous and heterogeneous microscopic pores and the methods adopted in the literature to model confined fluids.<br>  ➢ FTS in general, including: FTS chemistry, thermodynamic modeling of the reaction mixture and reaction product in bulk and in pores as well as the reaction kinetics.<br>  ➢ Utilization of supercritical fluids in FTS |
| **Task 2:** Understand the thermodynamic model for confined fluids that will be used. | • Understand the derivation of the EOS model from its principles and the assumptions used in each stage of derivation.<br>• Learn the implementation the EOS model on the specified case study (FTS reaction mixture). |

**Table 1**: Continued

| Task | Methodology |
|---|---|
| **Task 3:** Collect the experimental data required to use the EOS model and estimate its adjustable parameters. | • Collect adsorption experimental data that used to calculate the model's adjustable parameters.<br>• Understand the model sensitivity to system conditions and its applicability to different condition such as critical/supercritical conditions. |
| **Task 4:** Set up the phase behavior problem for FTS conditions. And conduct multi-phase equilibrium calculations for bulk and confining region within the catalyst. | • Set up the research problem which examined phase behavior of the FTS reaction mixture in the gas phase and in the supercritical phase.<br>• Identify appropriate product model for FTS reaction mixture.<br>• Extend the capabilities of Travalloni's EOS for the confined phase to typical FTS reaction mixture at different conversion levels.<br>• Conduct flash like calculations to determine the system's stability and investigate the nature of the phases in the bulk and in the confined pores. |

## 3.2 Development of Equation of State for Confined Fluids

The equation of state models can be derived from statistical mechanics, which is the branch of science that is used to describe the mechanical nature of a given system at a microscopic level by using mathematical models based on the probability theory. A common use of statistical mechanics is in explaining the thermodynamic behavior of large systems. It provides exact methods to connect thermodynamic quantities (such as heat capacity) to microscopic behavior, whereas in classical thermodynamics the only available option would be to tabulate data or use empirical correlations for such quantities for various materials. The branch of statistical mechanics that treats and extends classical thermodynamics is known as *statistical thermodynamics.*

15

In the case of an isolated system bounded in finite volume $V$, with temperature $T$, and total number of molecules $N$ in a pure fluid (or $N_1, N_2, .., N_{NC}$, for a mixture of NC components) as independent variables, the canonical partition function $Q$ represents the window between statistical and the classical thermodynamics, from which all the thermodynamic quantities such as Helmholtz free energy $A$ and pressure $P$ can be computed, as follows [24]:

$$A(T, V, N_1, N_2..N_{NC}) = -kT \ln Q(T, V, N_1, N_2..N_{NC}) \qquad (3.1)$$

$$P = kT \left( \frac{\partial (\ln Q)}{\partial V} \right)_{T, N_1, N_2, ... N_{NC}} \qquad (3.2)$$

where $k$ is the Boltzmann constant ( a physical constant relating energy at the individual particle level with temperature and it is equal to $= 1.3806488 \times 10^{-23}$ m$^2$ kg s$^{-2}$ K$^{-1}$). The equation of state model for confined fluids in porous media has been developed by Travalloni et al. [11, 12] based on the generalized van der Waals theory [24], in which the canonical partition function is given as:

$$Q(T, V, N_1, N_2, ... N_{NC}) = \prod_{i=1}^{NC} \left( \frac{q_i^{N_i}}{\lambda_i^{3N_i} N_i!} \right) V_f^N \exp \left( \int_{\infty}^{T} \frac{E_{conf}}{kT^2} dT \right) \qquad (3.3)$$

where index $i$ denotes a component, $q$ and $\lambda$ are intramolecular and translational contributions, respectively, $V_f$ is the free volume, and $E_{conf}$ is the configurational energy. The basis of several cubic EOS is to develop expressions for repulsive part of the equation of state, which is represented by $V_f$, and attractive part which, is represented by $E_{conf}$,

16

assuming the fluid molecules are hard spheres that interact with each other through one of the well-known interaction potential models and, in the present case, through the square-well potential [11, 12].

Complete derivation of the Peng-Robinson EOS extended to the confined fluids (PR-C) is provided elsewhere [11, 12] and given as follows:

$$P = \frac{RT}{v - b_p} - \frac{a_p}{v^2} - \theta \frac{b_p}{v^2} \left(1 - \frac{b_p}{v}\right)^{\theta - 1} \left(1 - F_{pa}\right) \left( RT \left(1 - \exp\left(-\frac{N_{av}\varepsilon_p}{RT}\right)\right) - N_{av}\varepsilon_p \right) \tag{3.4}$$

where $R$ is the universal gas constant, $v$ is the molar volume of the fluid mixture, $F_{pa}$ is a term represents the fraction of the confined molecules in the range of pore attractive field and their random distribution inside the pore, $\theta_i$ geometric factor and $N_{av}$ is the Avogadro number.

$b_p$ is the confinement-modified volume parameter of the fluid mixture:

$$b_p = \sum_{i=1}^{NC} x_i b_{p,i} \tag{3.5}$$

where $x_i$ is the mole fraction of component $i$ and $b_{p,i}$ is the confinement-modified volume parameter of pure component $i$:

$$b_{p,i} = \frac{N_{av}}{\rho_{\max,i}} \tag{3.6}$$

where $\rho_{max,i}$ is the packing density of pure component $i$. It depends on the molecule size and the pore size, and the procedure to estimate this property can be found in reference [12].

$a_p$ is the confinement-modified energy parameter of the fluid mixture:

$$a_p = \sum_{i=1}^{NC} \sum_{j=1}^{NC} \left( x_i x_j a_{p,ij} \right) \tag{3.7}$$

where $a_{p,ij}$ is given by the combination rule:

$$a_{p,ij} = \sqrt{a_i a_j} \left( 1 - \frac{2}{5} \frac{\sigma_{ij}}{r_p} \right) \tag{3.8}$$

and $a_i$ is the energy parameter of pure component $i$. Parameter $a_i$ is defined as:

$$\frac{\sqrt{2} N_{av}^2 \varepsilon_{ii}}{\rho_{max,i}} \alpha_{PR,i} (T) \tag{3.9}$$

where $\alpha_{PR,i}$ is the conventional functions of temperature and acentric factor for Peng-Robinson EOS. It is noteworthy to mention that the model is derived assuming that the pores are cylindrical with homogeneous surfaces [12].

The molecule–wall interaction parameters depend only on the chemical nature of the solid and of each fluid component, and can be fitted from experimental data of pure fluid adsorption. With estimated values for the molecule–wall interaction parameters of all fluid components, the model can be used in predictive calculations of mixture adsorption as will be further demonstrated in  section 3.4 [11, 12]. The extended model (Eq. 3.4) reduces to the respective bulk EOS in the limit of infinitely large pore size; therefore, they are valid for both confined and bulk fluids. This EOS model (Eq. 3.4) will be used for the phase behavior investigation in FTS.

### 3.3 Parameter Estimation

The characteristic size parameter $\delta_{p,i}$ and characteristic energy parameter $\varepsilon_{p,i}$ for the model has been estimated by fitting adsorption experimental data using XSEOS Thermodynamic computational package for Excel ® [25].The steps are summarized as follows:

1- Collect isothermal adsorption experimental data for pure components (adsorbed amount vs. pressure) and the adsorbent data (i.e. pore radius and specific pore volume).

2- Calculate the fugacity of the substance in the bulk phase using embedded XSEOS Peng-Robinson EOS for confined fluids assuming infinitely large pore and zero size and energy interaction parameters.

3- Calculate the fugacity of the substance in the adsorbed phase applying the embedded XSEOS Peng-Robinson EOS for confined fluids using the specified pore radius and initial estimates for size and energy interaction parameters.

4- Assume thermodynamic equilibrium between the bulk phase and adsorbed phase, which is same as assuming equal fugacities.

5- Calculate the adsorbed amount using the new characteristic parameters.

6- Minimize the sum of the squared differences between calculated and experimental adsorbed amounts using Solver ® by changing the characteristic parameters and adsorbed phase pressure, under the constrained that the fugacities in the bulk and confined phases are equal is objective functions is given as:

$$\left(M_{calculated} - M_{experimental}\right)^2 = 0 \tag{3.10}$$

where M (mol/kg), represents the adsorbed amount (moles) per kg adsorbent.

In the case of FTS adsorption on heterogeneous catalyst, the size parameter and the energy parameter were estimated for the reactants (carbon monoxide, hydrogen and solvent which is either nitrogen (gas phase) or hexane (SCF phase) and the products which will be water and $n$-alkanes represented by a mixture from $C_1$ to $C_8$. The representation is limited to $C_8$ because of the lack of adsorption experimental data for heavier hydrocarbons.

The calculated adsorption isotherms were found to be in good agreement with the experimental data as shown in Appendix A. The hydrogen and nitrogen parameters were fitted on zeolite A due to the lack of experimental data for adsorption on activated alumina and it was assumed that the behavior will be similar because of similarity of the chemical nature of zeolites and Activated Alumina. The hydrocarbon $C_1$- $C_5$ and $C_8$  parameters were fitted to activated alumina, and good fitting was obtained (see Appendix A). The hydrocarbons $C_6$ and $C_7$ parameter were estimated via linear interpolation. It has been found that interpolated parameter resulted in a similar trend as the parameters estimated by fitting experimental data as demonstrated in Figure 2. The parameters estimated and used in this study are listed in Table 2.
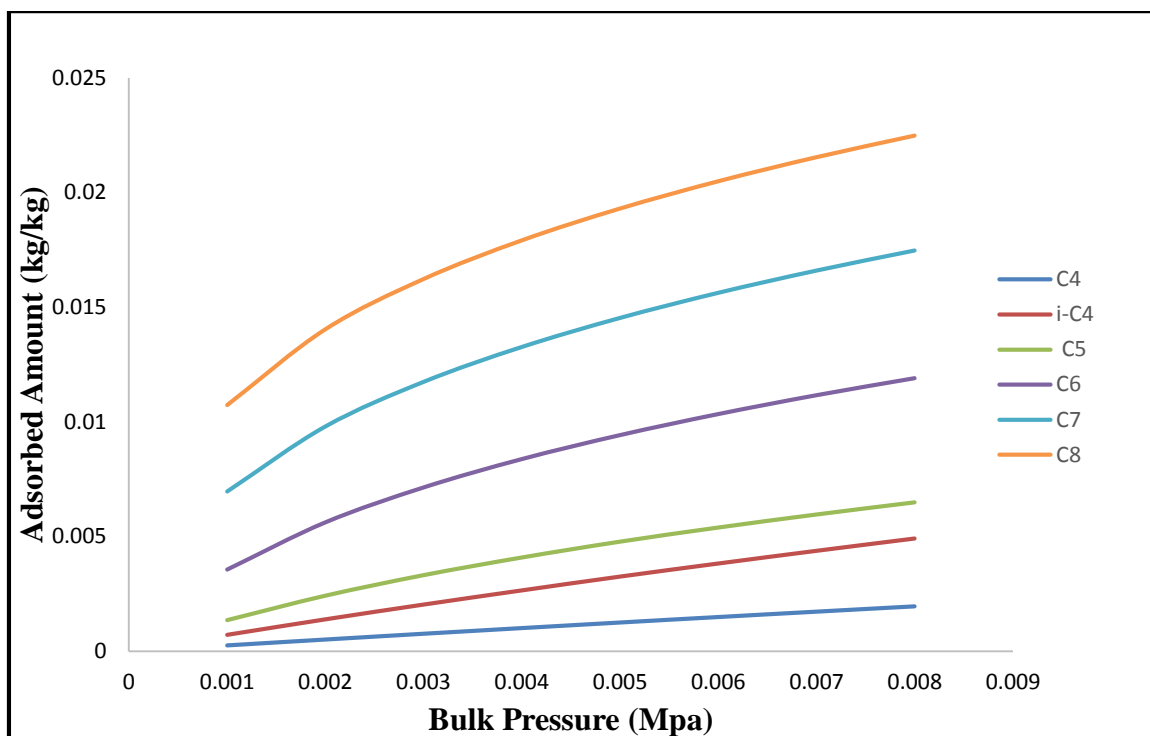
**Figure 2:** Adsorption isotherms on activated alumina at 313.15 K

**Table 2 :** Size and energy wall interaction parameters

| Component | $\varepsilon_P/k$ | $\delta_P/\sigma$ |
|---|---|---|
| Carbon monoxide | 1390.815 | 0.52496 |
| hydrogen | -2119.972 | 1.23054 |
| Nitrogen | 3112.913 | 0.12109 |
| Water | 5082.668 | 0.98135 |
| $C_1$ | 798.024 | 0.8804 |
| $C_2$ | 1026.135 | 0.798 |
| $C_3$ | 1254.245 | 0.7156 |
| $C_4$ | 1279.653 | 0.3481 |
| $C_5$ | 1797.517 | 0.1779 |
| $C_6$ | 2137.662 | 0.1558 |
| $C_7$ | 2477.808 | 0.1338 |
| $C_8$ | 2817.953 | 0.1117 |

**3.4 Multiphase Equilibrium Calculations & Phase Characterization of FTS Reaction Mixture**

The catalytic reactions usually occur at the catalyst pore surface whereby active sites exit. The reaction sequence starts with adsorption of the reactants (CO, $H_2$ and solvent in case of SCF-FTS) and ends with desorption of products (series of hydrocarbons and water). Instantaneously along the reactor bed, the catalyst pores will be confining the products mixture and fractions of the reactants which depend on the reaction conversion. In the current study, a multiphase equilibrium calculation algorithm [26] was adapted for using the PR-C EOS. The specifications are the system temperature, the total amount of each fluid component, the total volume of the bulk region and of each confining region, and the pore size and adsorption energy distributions (i.e., the pore radius and the pair of molecule-wall interaction parameters assigned to each confining region). With these specifications, the thermodynamic equilibrium condition is the minimum Helmholtz energy (A) of the system [11, 26]:

$$A = \sum_{g=1}^{NR} \sum_{h=1}^{NF_g} A_{gh} \tag{3.11}$$

where $NR$ is the total number of regions available to the fluid (including the bulk region), $NF_g$ is the number of fluid phases in region $g$, and $A_{gh}$ is the Helmholtz energy of phase $h$ in region $g$. The contribution of each phase (bulk or confined) to $A$ was obtained from the PR-C model (Eq. 3.4) by [11]:

$$A_{gh} = -P_{gh}V_{gh} + \sum_{i=1}^{NC} n_{gh,i} \mu_{gh,i} \qquad (3.12)$$

where $P_{gh}$ and $V_{gh}$ are the pressure and the volume of phase $h$ in region $g$, respectively, and $n_{gh,i}$ and $\mu_{gh,i}$ are the mole number and the chemical potential of component $i$ in the same phase, respectively.

The Helmholtz energy has been minimized using a Newton method based algorithm, developed by Murray [27], with variables related to the volume of each phase and to the amount of each component in each phase. Details of the multi-phase calculation for the adsorption problem are provided in the references [11, 26].

The multiphase equilibrium algorithm developed by Travalloni et al.[11] was set up in such a way that the specifications are the system temperature $T$, the total amount of each fluid component $N_i$, the total volume of the bulk region $V_{bulk}$, and of the confining region $V_{pore}$, and the pore size and adsorption energy distributions (i.e., the pore radius and the pair of molecule-wall interaction parameters assigned to the confining region) $\delta_{p,i}$, $\varepsilon_{p,i}$, the pressure, and the amount and the composition of each phase (bulk/confined) are calculated. In the case of modeling the FT phase behavior the total pressure was kept constant and was set to 80 bar for SCF-FTS and 20 bar for gas phase FTS. The specifications of the simulation study are given in Table 3. The total initial amount of moles of the FTS mixture was varied by trial and error for SCF-FTS operating pressure of 80 bar and gas phase FTS operating pressure of 20 bar. The calculations have been done

under the constraint of the constant bulk volume and the molar mass of the mixture as follows:

$$\frac{V_{Bulk}}{M_W} = \frac{N_T}{\rho_{Bulk}} = \alpha \qquad (3.13)$$

where $M_W$ is the mixture molar mass, $N_T$ is the initial total number of moles, $\rho_{Bulk}$ is the initial bulk density and $\alpha$ is constant ratio between the bulk volume and the mixture molecular weight. Once the total number of moles is calculated, the initial amount of each component can be determined according to their stoichiometric mole fractions.

The first set of the equilibrium calculation considers FTS mixture in the conventional gas phase at 20 bar and 513 K. The mixture is composed of carbon monoxide, hydrogen, water and hydrocarbons from $C_1$ to $C_8$. The mole fractions were calculated from the reaction stoichiometric ratios at different conversions (X= 25%, 50% and 75 %), the hydrocarbon fractions were calculated using the ASF product distribution model the FTS product distribution (Eq. 1.2) as shown in Table 4.

**Table 3 :** Specifications of the simulation study

| Temperature (K) | 513 |
|---|---|
| Pressure (bar) | 20 (for gas phase FTS) or 80 (for SCF-FTS) |
| Tube Diameter (cm) | 1.52 |
| Bed length (cm) | 3.00 |
| Bed porosity | 0.40 |
| Total Pore volume (cm$^3$/g) | 1.14 |
| Packing density (cm$^3$/g) | 0.40 |
| Pore radius (A) | 68.57 |
| Data Calculated[1] | |
| Reactor Volume (m$^3$) | 5.47E-06 |
| Volume of Bulk (m$^3$) | 2.19E-06 |
| Volume of Pores (m$^3$) | 2.48E-06 |

**Table 4 :** Stoichiometric mole fractions in gas phase reaction at 20 bar

| Component | X= 25% | X= 50% | X= 75% |
|---|---|---|---|
| Carbon monoxide | 0.3 | 0.25 | 0.1667 |
| Hydrogen | 0.5632 | 0.4081 | 0.1496 |
| Water | 0.1 | 0.25 | 0.5 |
| $C_1$ | 0.0201 | 0.0504 | 0.1007 |
| $C_2$ | 0.002 | 0.0049 | 0.0098 |
| $C_3$ | 0.0027 | 0.0068 | 0.0135 |
| $C_4$ | 0.003 | 0.0076 | 0.0152 |
| $C_5$ | 0.0029 | 0.0073 | 0.0146 |
| $C_6$ | 0.0025 | 0.0062 | 0.0124 |
| $C_7$ | 0.0019 | 0.0047 | 0.0094 |
| $C_8$ | 0.0016 | 0.0041 | 0.0081 |

[1] The reactor volume has been calculated as the volume of cylindrical tube = $\Pi r^2 L$.
The bulk volume = bed porosity*reactor volume
The pore volume = total pore volume*packing density*reactor volume.

The second set of calculations dealt with the simultaneous assessment for the gas phase FTS reaction mixture and SCF phase FTS reaction mixture in which the pressure was set to 80 bar. The reaction starts with a mixture of syngas and solvent in terms of molar ratio 1:3. The solvent is considered as inert in the reaction and it was chosen to be nitrogen in the case of gas phase and hexane in the of SCF phase [28]. The partial pressure of the syngas at the reactor entrance is 20 bar and the solvent is 60 bar. At each conversion the mole fractions have been calculated and their values shown in Table 5.

**Table 5 :** Stoichiometric mole fractions in gas phase and SCF phase reaction at 80 bar

| Component | Conversion X = 25% | | Conversion X = 50% | | Conversion X = 75% | |
|---|---|---|---|---|---|---|
| | *Gas phase* | *SCF phase* | *Gas phase* | *SCF phase* | *Gas phase* | *SCF phase* |
| **Carbon monoxide** | 0.0652 | 0.0652 | 0.0455 | 0.0455 | 0.0238 | 0.0238 |
| **Hydrogen** | 0.1224 | 0.1247 | 0.0742 | 0.079 | 0.0214 | 0.0289 |
| **Solvent** | 0.7826 | 0.7826 | 0.8182 | 0.8182 | 0.8571 | 0.8571 |
| **Water** | 0.0217 | 0.0217 | 0.0455 | 0.0455 | 0.0714 | 0.0714 |
| $C_1$ | 0.0044 | 0.0015 | 0.0092 | 0.0031 | 0.0144 | 0.0048 |
| $C_2$ | 0.0004 | 0.0005 | 0.0009 | 0.001 | 0.0014 | 0.0016 |
| $C_3$ | 0.0006 | 0.0007 | 0.0012 | 0.0014 | 0.0019 | 0.0022 |
| $C_4$ | 0.0007 | 0.0008 | 0.0014 | 0.0016 | 0.0022 | 0.0025 |
| $C_5$ | 0.0006 | 0.0007 | 0.0013 | 0.0016 | 0.0021 | 0.0024 |
| $C_6$ | 0.0005 | 0.0007 | 0.0011 | 0.0014 | 0.0018 | 0.0022 |
| $C_7$ | 0.0004 | 0.0005 | 0.0009 | 0.0011 | 0.0013 | 0.0017 |
| $C_8$ | 0.0004 | 0.0004 | 0.0007 | 0.0008 | 0.0012 | 0.0012 |

# 4.  RESULTS AND DISCUSSION

This chapter covers the outcome of our multiphase equilibrium calculations for the confined phase of FTS reaction mixture. The first section highlights the main results for the conventional gas phase reaction at 20 bar in terms of mole fraction distribution in both the bulk phase (inter-particle) and confined phase (intra-particle). The reaction mixture both in the bulk phase and inside the catalyst pores (confined phase) for the gas-phase FTS has been considered as hydrocarbon products, remaining syngas and water. The second section presents the results of inter-particle/intra-particle assessments for a mixture of syngas co-fed with inert solvent (nitrogen/hexane), water and hydrocarbons at high pressure of 80 bar. This purpose of this assessment is to address and compare the characteristics of the confined phase of FTS reaction mixture in both the SCF phase and in the gas phase FTS.

## 4.1 Multiphase Equilibrium for FTS Mixture at 20 bar

### 4.1.1 Conventional Gas Phase at 20 bar

The conventional gas phase system was represented as a mixture of syngas (reactants), water and hydrocarbons (products) at 20 bar and 513 K. Three cases were studied, at conversion of 25%, 50% and 75% their results are summarized in Tables 6-8 and Figures 3-5.

For 25% conversion (Table 6 and Figure 3) the model has predicted that the mole fraction of hydrogen is equal to 0.6222 in the pore phase is and 2.28E-6 in the bulk region.

Similar prediction patterns were predicted at 50% and 75%, but with smaller mole fractions of hydrogen because it is a reactant in FTS (see Tables 7 and 8).

On the other hand for 25% conversion 92 mol % of the mixture existing in the bulk phase is carbon monoxide. Similar phenomena appeared where carbon monoxide represents 79 mol% (for X=0.5) and 43mol% (for X=0.75) from the mixture in the bulk phase as shown in Tables 6-8. This preferential adsorption of hydrogen can be attributed to its small molecules which make it easier for hydrogen molecules to enter the pore space especially in the high pressure conditions that the molecule are experiencing in the confined space.

It can also be seen from Figure 3 that 11 mol% of the mixture in the pore phase is water (for X=0.25), and increasing fraction of water equals to 27 mol% and 53 mol% in the adsorbed phase as the conversion X increases to 50% and 75% respectively (as shown in Figures 3 and 4). Due to the high pressure and temperature conditions in the bulk phase and in the adsorbed phase, the mixture in each region is homogenous (miscible gases in one another) with low density (gas-like) and high compressibility factor as outlined in Tables 6-8. Moreover, our model predicts that for all conversion the hydrocarbons from $C_5$ to $C_8$ are existing in the pore in a considerable amounts with respect to their initial amounts due to their preferential adsorption (see Figures 3, 4, and 5).

Although explained in section 3.4, it is worth mentioning that the global amounts in Tables 6-8 (as well as 9-14) represents the molar components amounts and the corresponding mole fractions were computed for each conversion. These component

amounts were scaled by trial and error in such a way that the bulk pressure equal to 20 bar (or 80 bar in the following sections).
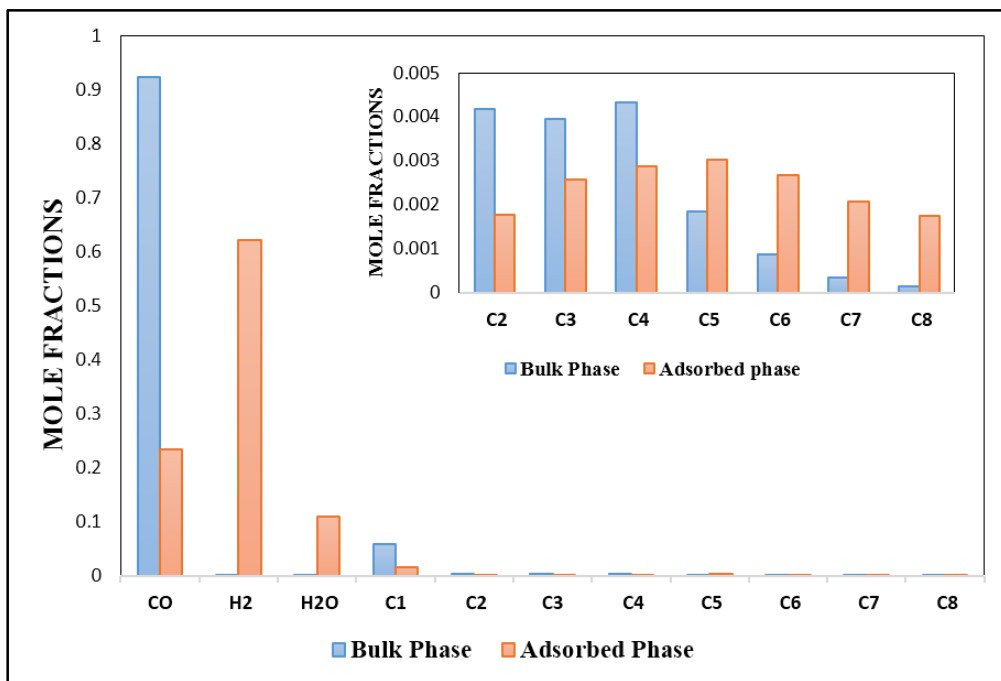


**Figure 3:** Bulk and confined phase molar composition at 25% conversion, 513 K and 20 bar

**Table 6 :** Global, bulk, and confined phase configuration at 25% conversion, 513 K and 20 bar

| Phase | Global | Bulk Phase | Adsorbed Phase |
|---|---|---|---|
| **Compressibility Z** | - | 1.01 | 10.97 |
| **Density (kg/m³)** | 63.00[2] | 12.91 | 50.38 |
| **Total Amount** | 1.04E-02 | 9.87E-04 | 9.43E-03 |
| **Component** | **Amount (moles)** | **Amount (moles)** | **Amount (moles)** |
| **Carbon monoxide** | 3.12E-03 | 9.13E-04 | 2.21E-03 |
| **Hydrogen** | 5.87E-03 | 2.25E-09 | 5.87E-03 |
| **Water** | 1.04E-03 | 4.75E-07 | 1.04E-03 |
| $C_1$ | 2.09E-04 | 5.86E-05 | 1.51E-04 |
| $C_2$ | 2.08E-05 | 4.11E-06 | 1.67E-05 |
| $C_3$ | 2.81E-05 | 3.90E-06 | 2.42E-05 |
| $C_4$ | 3.12E-05 | 4.27E-06 | 2.70E-05 |
| $C_5$ | 3.02E-05 | 1.82E-06 | 2.84E-05 |
| $C_6$ | 2.60E-05 | 8.50E-07 | 2.52E-05 |
| $C_7$ | 1.98E-05 | 3.38E-07 | 1.95E-05 |
| $C_8$ | 1.67E-05 | 1.49E-07 | 1.65E-05 |

---

[2] Mass of fluid divided by bulk phase volume

**Figure 4 :** Bulk and confined phase molar composition at 50% conversion, 513 K and 20 bar

**Table 7 :** Global, bulk, and confined phase configuration at 50% conversion, 513 K and 20 bar

| Phase | Global | Bulk Phase | Adsorbed Phase |
|---|---|---|---|
| **Compressibility Z** | - | 1.0042 | 7.7106 |
| **Density (kg/m³)** | 84.00³ | 12.58 | 71.40 |
| **Total Amount** | 1.15E-02 | 1.02E-03 | 1.04E-02 |
| **Component** | **Amount (moles)** | **Amount (moles)** | **Amount (moles)** |
| **Carbon monoxide** | 2.87E-03 | 7.92E-01 | 1.97E-01 |
| **Hydrogen** | 4.68E-03 | 9.36E-09 | 4.48E-01 |
| **Water** | 2.87E-03 | 1.08E-02 | 2.73E-01 |
| **$C_1$** | 5.78E-04 | 1.60E-01 | 3.97E-02 |
| **$C_2$** | 5.62E-05 | 1.00E-02 | 4.40E-03 |
| **$C_3$** | 7.80E-05 | 9.44E-03 | 6.54E-03 |
| **$C_4$** | 8.71E-05 | 1.02E-02 | 7.35E-03 |
| **$C_5$** | 8.37E-05 | 4.40E-03 | 7.58E-03 |
| **$C_6$** | 7.11E-05 | 2.00E-03 | 6.61E-03 |
| **$C_7$** | 5.39E-05 | 7.62E-04 | 5.09E-03 |
| **$C_8$** | 4.70E-05 | 3.45E-04 | 4.47E-03 |

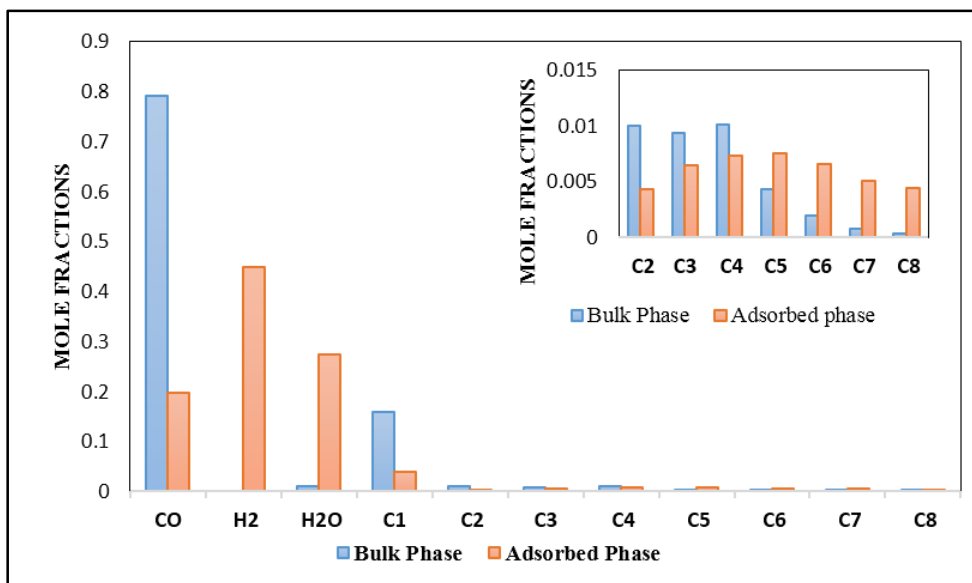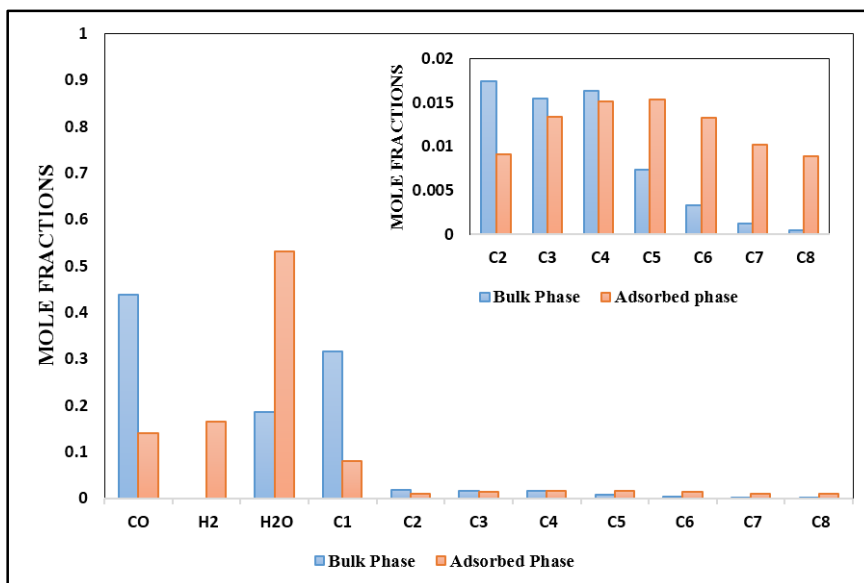³ Mass of fluid divided by bulk phase volume

**Figure 5 :** Bulk and confined phase molar composition at 75% conversion, 513 K and 20 bar

**Table 8 :** Global, bulk, and confined phase configuration at 75% conversion, 513 K and 20 bar

| Phase | Global | Bulk Phase | Adsorbed Phase |
|---|---|---|---|
| **Compressibility Z** | - | 0.99 | 3.36 |
| **Density (kg/m$^3$)** | 113.70[4] | 11.26 | 98.88 |
| **Total Amount** | 1.16E-02 | 1.03E-03 | 1.06E-02 |
| **Component** | **Amount (moles)** | **Amount (moles)** | **Amount (moles)** |
| **Carbon monoxide** | 1.94E-03 | 4.53E-04 | 1.49E-03 |
| **Hydrogen** | 1.74E-03 | 1.46E-19 | 1.74E-03 |
| **Water** | 5.82E-03 | 1.91E-04 | 5.63E-03 |
| **$C_1$** | 1.17E-03 | 3.26E-04 | 8.47E-04 |
| **$C_2$** | 1.14E-04 | 1.80E-05 | 9.61E-05 |
| **$C_3$** | 1.57E-04 | 1.59E-05 | 1.41E-04 |
| **$C_4$** | 1.77E-04 | 1.69E-05 | 1.60E-04 |
| **$C_5$** | 1.70E-04 | 7.61E-06 | 1.62E-04 |
| **$C_6$** | 1.44E-04 | 3.40E-06 | 1.41E-04 |
| **$C_7$** | 1.09E-04 | 1.23E-06 | 1.08E-04 |
| **$C_8$** | 9.43E-05 | 5.36E-07 | 9.38E-05 |

---

[4] Mass of fluid divided by bulk phase volume

**4.2 Multiphase Equilibrium for FTS mixture at 80 bar**

*4.2.1 Gas Phase at 80 bar*

The gas phase reaction mixture in this case is composed of syngas and nitrogen as inert (in a molar ratio 1:3) besides water and hydrocarbon products at 80 bar and 513 K. It can be seen from Figure 6 that in this case unlike the conventional gas phase (section 4.1.1 and Figure 3-5) that carbon monoxide tends to exist in a greater portion in the adsorbed phase than in the bulk phase. On the other hand, similar phenomena appearing for the hydrogen that found to mostly exist in the adsorbed phase with negligible amount in the bulk phase. Nitrogen is an inert in the reaction that does not depend on the conversion level and it dominates the bulk phase as it represent 97 mol% and 65 mol% of the adsorbed phase (Figures 6-8). As shown in Tables 9-11 water and hydrocarbon exist in the confined phase in greater amounts than the bulk with respect to their initial amounts. The bulk phase and the adsorbed phase have almost similar low and gas-like densities.
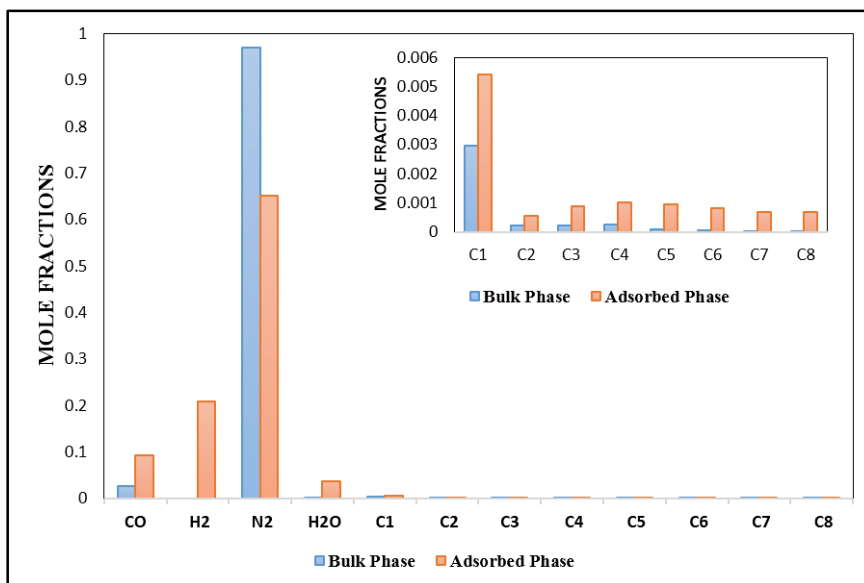
**Figure 6 :** Bulk and confined phase molar compositions at 25% conversion, 513 K and 80 bar

**Table 9 :** Global, bulk, and confined phase configuration at 25% conversion, 513 K and 80 bar

| Phase | Global | Bulk Phase | Adsorbed Phase |
|---|---|---|---|
| **Compressibility Z** | - | 1.03 | 3.21 |
| **Density (kg/m³)** | 109.45[5] | 51.13 | 56.04 |
| **Total Amount** | 9.69E-03 | 3.99E-03 | 5.70E-03 |
| **Component** | **Amount (moles)** | **Amount (moles)** | **Amount (moles)** |
| **Carbon monoxide** | 6.32E-04 | 1.02E-04 | 5.29E-04 |
| **Hydrogen** | 1.19E-03 | 1.84E-21 | 1.19E-03 |
| **Nitrogen** | 7.58E-03 | 3.88E-03 | 3.71E-03 |
| **Water** | 2.10E-04 | 3.16E-08 | 2.10E-04 |
| $C_1$ | 4.26E-05 | 1.18E-05 | 3.08E-05 |
| $C_2$ | 3.88E-06 | 7.96E-07 | 3.08E-06 |
| $C_3$ | 5.81E-06 | 8.56E-07 | 4.96E-06 |
| $C_4$ | 6.78E-06 | 9.96E-07 | 5.79E-06 |
| $C_5$ | 5.81E-06 | 3.69E-07 | 5.45E-06 |
| $C_6$ | 4.85E-06 | 1.67E-07 | 4.68E-06 |
| $C_7$ | 3.88E-06 | 7.05E-08 | 3.81E-06 |
| $C_8$ | 3.88E-06 | 3.72E-08 | 3.84E-06 |

---

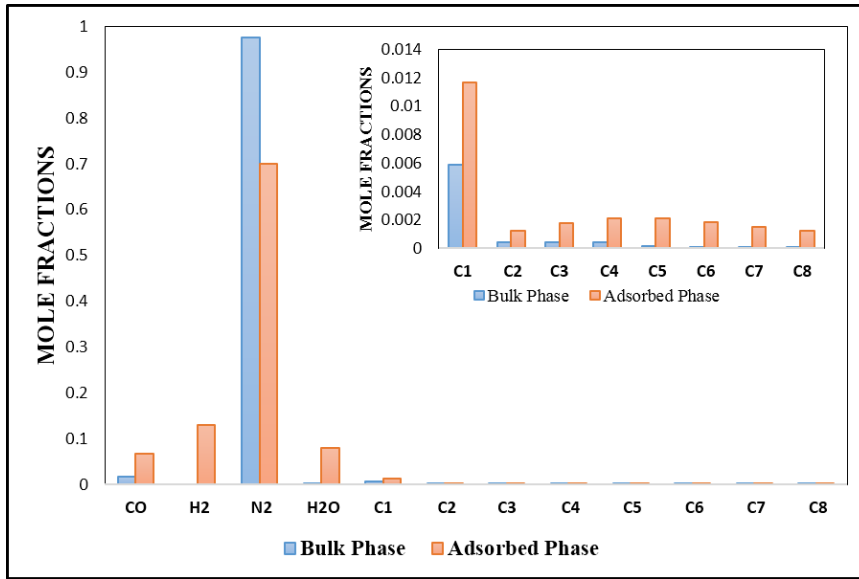[5] Mass of fluid divided by bulk phase volume

**Figure 7 :** Bulk and confined phase molar compositions at 50% conversion, 513 K and 80 bar

**Table 10 :** Global, bulk, and confined phase configuration at 50% conversion, 513 K and 80 bar

| Phase | Global | Bulk Phase | Adsorbed Phase |
|---|---|---|---|
| **Compressibility Z** | - | 1.03 | 3.21 |
| **Density (kg/m$^3$)** | 110.10$^6$ | 51.08 | 56.36 |
| **Total Amount** | 9.33E-03 | 3.99E-03 | 5.33E-03 |
| **Component** | **Amount (moles)** | **Amount (moles)** | **Amount (moles)** |
| **Carbon monoxide** | 4.24E-04 | 6.31E-05 | 3.61E-04 |
| **Hydrogen** | 6.92E-04 | 2.53E-23 | 6.92E-04 |
| **Nitrogen** | 7.63E-03 | 3.90E-03 | 3.73E-03 |
| **Water** | 4.24E-04 | 8.85E-08 | 4.24E-04 |
| **C$_1$** | 8.58E-05 | 2.36E-05 | 6.22E-05 |
| **C$_2$** | 8.39E-06 | 1.69E-06 | 6.70E-06 |
| **C$_3$** | 1.12E-05 | 1.61E-06 | 9.58E-06 |
| **C$_4$** | 1.31E-05 | 1.87E-06 | 1.12E-05 |
| **C$_5$** | 1.21E-05 | 7.51E-07 | 1.14E-05 |
| **C$_6$** | 1.03E-05 | 3.43E-07 | 9.92E-06 |
| **C$_7$** | 8.39E-06 | 1.48E-07 | 8.24E-06 |
| **C$_8$** | 6.53E-06 | 5.97E-08 | 6.47E-06 |

---

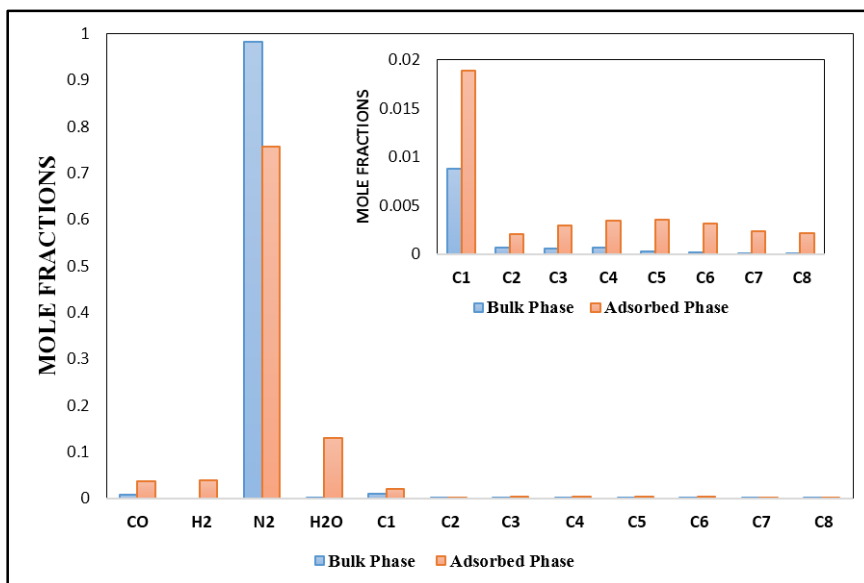[6] Mass of fluid divided by bulk phase volume

**Figure 8 :** Bulk and confined phase molar compositions at 75% conversion, 513K and 80 bar

**Table 11 :** Global, bulk, and confined phase configuration at 75% conversion, 513 K and 80 bar

| Phase | Global | Bulk Phase | Adsorbed Phase |
|---|---|---|---|
| **Compressibility Z** | - | 1.03 | 2.52 |
| **Density (kg/m³)** | 110.80[7] | 51.10 | 56.66 |
| **Total Amount** | 8.96E-03 | 4.00E-03 | 4.96E-03 |
| **Component** | Amount (moles) | Amount (moles) | Amount (moles) |
| **Carbon monoxide** | 2.13E-04 | 2.88E-05 | 1.84E-04 |
| **Hydrogen** | 1.92E-04 | 1.25E-25 | 1.92E-04 |
| **Nitrogen** | 7.68E-03 | 3.92E-03 | 3.75E-03 |
| **Water** | 6.40E-04 | 1.83E-07 | 6.39E-04 |
| $C_1$ | 1.29E-04 | 3.53E-05 | 9.37E-05 |
| $C_2$ | 1.25E-05 | 2.49E-06 | 1.01E-05 |
| $C_3$ | 1.70E-05 | 2.39E-06 | 1.46E-05 |
| $C_4$ | 1.97E-05 | 2.74E-06 | 1.70E-05 |
| $C_5$ | 1.88E-05 | 1.14E-06 | 1.77E-05 |
| $C_6$ | 1.61E-05 | 5.24E-07 | 1.56E-05 |
| $C_7$ | 1.16E-05 | 1.97E-07 | 1.14E-05 |
| $C_8$ | 1.07E-05 | 9.50E-08 | 1.07E-05 |

[7] Mass of fluid divided by bulk phase volume

*4.2.2 Supercritical Phase at 80 bar*

The supercritical phase reaction mixture in this case is composed of syngas and hexane as inert in a molar ratio 1:3 besides water and hydrocarbon products at 80 bar and 513 K. As outlined in Tables 12-14 the densities of both the bulk phase and the adsorbed phase have the same order of magnitude. Another observation from the same tables is that the reaction mixture inside the catalyst pore has vapor characteristics under the high pressure and relatively high temperature conditions, as expressed in terms of the calculated compressibility factor which was found to be 2.9 for X= 25%, 1.7 for X=50% and 0.89 for X=75%. On the other hand, the bulk phase showed vapor-like densities independent of the conversion with compressibility factor equivalent to 0.4. The densities observed in the bulk/confined phases for the SCF-FTS representative mixture were found to be much greater than those observed in the gas phase reaction (section 4.2.1 and Tables 9-11), which can be attributed to the dominating effect of the solvent hexane in the mixture. In addition, the solvent provides great heat dissipation that generated from the exothermic reaction. In agreement with the aforementioned statement Fan et al.[29] reported that the temperature rise in the supercritical FTS reactor bed is less than that of the gas phase FTS. Heat buffering in the SCF-FTS helped in preventing local overheat "hotspot formation" that leads to catalyst deactivation as reported by Elbashir et al.[16]. Furthermore the existence of dense vapor phase in the pore will provide greater diffusivity of the reactants. Preferential adsorption for hydrogen, water and hydrocarbons from $C_1$ to $C_8$ was observed under all conversions as shown in Figures 9-11. Moreover hydrogen is found to exist in the pore phase and negligibly in the bulk phase.
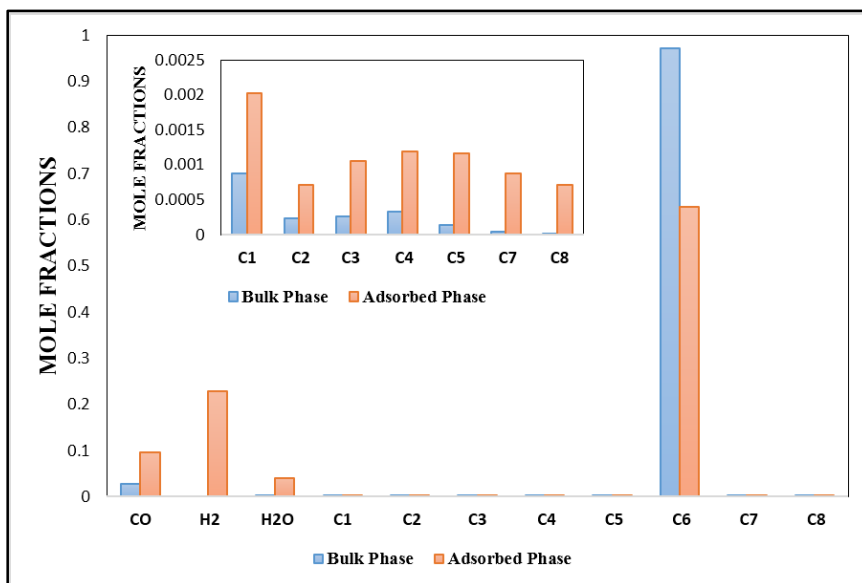
**Figure 9 :** Bulk and confined phase molar compositions at 25% conversion, 513 K and 80 bar

**Table 12 :** Global, bulk, and confined phase configuration at 25% conversion, 513 K and 80 bar

| Phase | Global | Bulk Phase | Adsorbed Phase |
|---|---|---|---|
| **Compressibility Z** | - | 0.40 | 2.97 |
| **Density (kg/m$^3$)** | 729.00[8] | 397.09 | 302.59 |
| **Total Amount** | 2.27E-02 | 1.03E-02 | 1.24E-02 |
| **Component** | Amount (moles) | Amount (moles) | Amount (moles) |
| **Carbon monoxide** | 1.48E-03 | 2.75E-04 | 1.21E-03 |
| **Hydrogen** | 2.83E-03 | 2.18E-16 | 2.83E-03 |
| **Water** | 4.93E-04 | 1.51E-07 | 4.93E-04 |
| **$C_1$** | 3.41E-05 | 8.95E-06 | 2.51E-05 |
| **$C_2$** | 1.14E-05 | 2.47E-06 | 8.89E-06 |
| **$C_3$** | 1.59E-05 | 2.73E-06 | 1.32E-05 |
| **$C_4$** | 1.82E-05 | 3.42E-06 | 1.47E-05 |
| **$C_5$** | 1.59E-05 | 1.49E-06 | 1.44E-05 |
| **$C_6$** | 1.78E-02 | 9.99E-03 | 7.80E-03 |
| **$C_7$** | 1.14E-05 | 3.87E-07 | 1.10E-05 |
| **$C_8$** | 9.08E-06 | 1.81E-07 | 8.90E-06 |

---

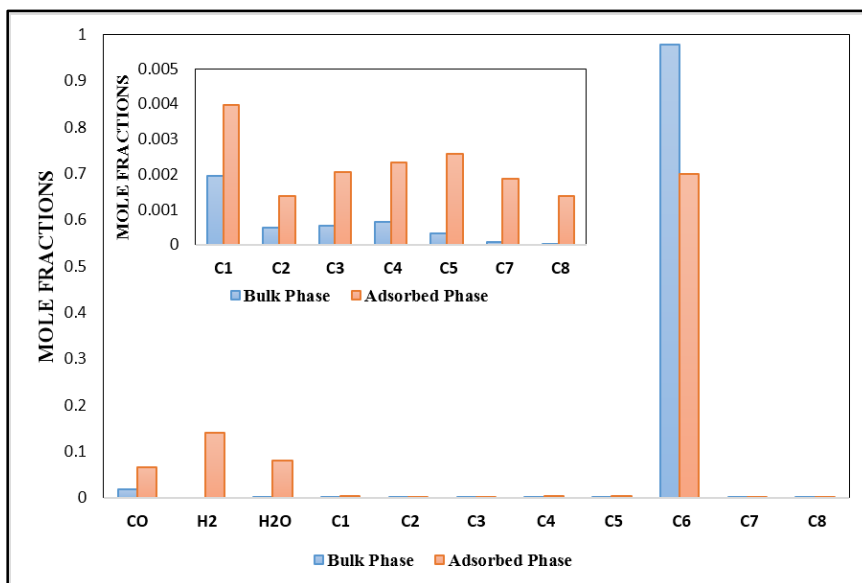[8] Mass of fluid divided by bulk phase volume

**Figure 10 :** Bulk and confined phase molar compositions at 50% conversion, 513 K and 80 bar

**Table 13 :** Global, bulk, and confined phase configuration at 50% conversion, 513 K and 80 bar

| Phase | Global | Bulk Phase | Adsorbed Phase |
|---|---|---|---|
| **Compressibility Z** | - | 0.40 | 1.70 |
| **Density (kg/m³)** | 798.90[9] | 400.81 | 361.78 |
| **Total Amount** | 2.38E-02 | 1.03E-02 | 1.35E-02 |
| **Component** | **Amount (moles)** | **Amount (moles)** | **Amount (moles)** |
| **Carbon monoxide** | 1.08E-03 | 1.93E-04 | 8.90E-04 |
| **Hydrogen** | 1.88E-03 | 3.62E-19 | 1.88E-03 |
| **Water** | 1.08E-03 | 7.22E-07 | 1.08E-03 |
| $C_1$ | 7.38E-05 | 2.02E-05 | 5.36E-05 |
| $C_2$ | 2.38E-05 | 5.14E-06 | 1.87E-05 |
| $C_3$ | 3.33E-05 | 5.53E-06 | 2.78E-05 |
| $C_4$ | 3.81E-05 | 6.77E-06 | 3.13E-05 |
| $C_5$ | 3.81E-05 | 3.36E-06 | 3.47E-05 |
| $C_6$ | 1.95E-02 | 1.01E-02 | 9.41E-03 |
| $C_7$ | 2.62E-05 | 8.07E-07 | 2.54E-05 |
| $C_8$ | 1.90E-05 | 3.30E-07 | 1.87E-05 |

---

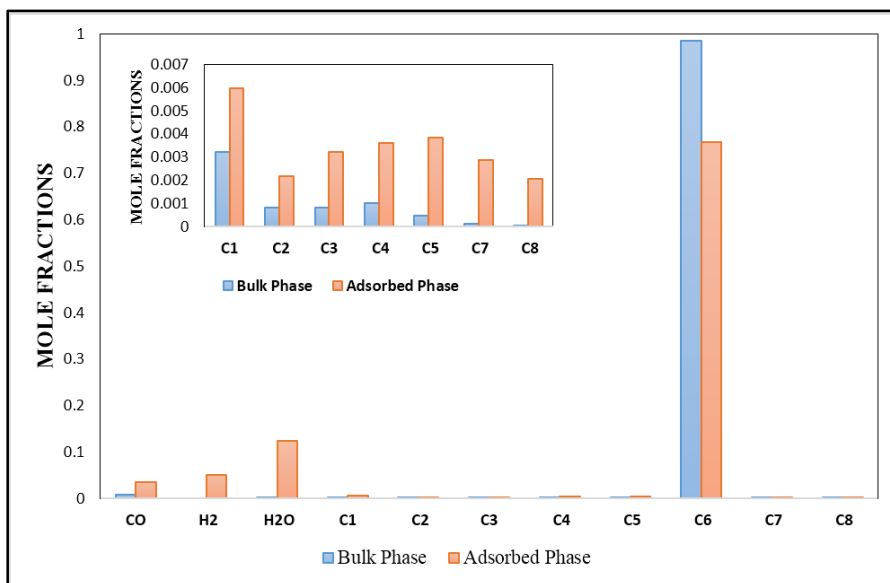[9] Mass of fluid divided by bulk phase volume

**Figure 11:** Bulk and confined phase molar compositions at 75% conversion, 513 K and 80 bar

**Table 14 :** Global, bulk, and confined phase configuration at 75% conversion, 513 K and 80 bar

| Phase | Global | Bulk Phase | Adsorbed Phase |
|---|---|---|---|
| **Compressibility Z** | - | 0.40 | 0.89 |
| **Density (Kg/m³)** | 857.50[10] | 404.99 | 410.19 |
| **Total Amount** | 2.44E-02 | 1.04E-02 | 1.40E-02 |
| **Component** | **Amount (moles)** | **Amount (moles)** | **Amount (moles)** |
| **Carbon monoxide** | 5.81E-04 | 9.37E-05 | 4.87E-04 |
| **Hydrogen** | 7.05E-04 | 2.88E-23 | 7.05E-04 |
| **Water** | 1.74E-03 | 2.63E-06 | 1.74E-03 |
| $C_1$ | 1.17E-04 | 3.33E-05 | 8.38E-05 |
| $C_2$ | 3.90E-05 | 8.48E-06 | 3.06E-05 |
| $C_3$ | 5.37E-05 | 8.78E-06 | 4.49E-05 |
| $C_4$ | 6.10E-05 | 1.05E-05 | 5.05E-05 |
| $C_5$ | 5.85E-05 | 5.02E-06 | 5.35E-05 |
| $C_6$ | 2.10E-02 | 1.02E-02 | 1.07E-02 |
| $C_7$ | 4.15E-05 | 1.22E-06 | 4.02E-05 |
| $C_8$ | 2.93E-05 | 4.70E-07 | 2.88E-05 |

---

[10] Mass of fluid divided by bulk phase volume

**4.3 Effects of Bulk Phase Density on the SCF-FTS**

In this section the effect of pressure on the supercritical phase FTS was investigated. Table 15 summarizes the results. In it, the first column is the specified bulk phase density assuming the pores are empty, and the second column is the bulk phase density at equilibrium. At low specified bulk densities, there are one bulk phase and one adsorbed phase, and it is observed that the equilibrium bulk density and pressure increases as the specified bulk density increases. At a specified bulk density of about 511.2 kg/m$^3$, an additional adsorbed phase appears in the system, accompanied by sharp decrease in the equilibrium bulk density and pressure.

At a specified bulk density of 703 kg/m$^3$, the second phase in the pores disappears, and the phase remaining in the pores in compressed and dense. This is can be attributed to the migration of the bulk material to the pore to form this new phase. Further increase in the bulk density results in pressure decrease to form a compressed and denser single phase inside the catalyst pore.

**Table 15 :** Effect of Bulk phase density on the SCF-FTS at X= 25% and 513 K

| Specifications | Results | | |
|---|---|---|---|
| Bulk Density (kg/m³) | Equilibrium Bulk Density (kg/m³) | Bulk Pressure (bar) | Observations |
| 480.00 | 394.83 | 65.86 | 1 bulk, 1 adsorbed phases |
| 500.00 | 394.88 | 73.76 | 1 bulk, 1 adsorbed phases |
| 511.00 | 402.14 | 78.30 | 1 bulk, 1 adsorbed phases |
| 511.20 | 383.37 | 67.81 | 1 bulk, 2 adsorbed phases |
| 511.30 | 383.38 | 67.82 | 1 bulk, 2 adsorbed phases |
| 680.00 | 398.03 | 79.34 | 1 bulk, 2 adsorbed phases |
| 700.00 | 399.63 | 80.80 | 1 bulk, 2 adsorbed phases |
| 701.00 | 399.71 | 80.87 | 1 bulk, 2 adsorbed phases |
| 702.00 | 399.79 | 80.95 | 1 bulk, 2 adsorbed phases |
| 703.00 | 387.62 | 74.03 | 1 bulk, 1 adsorbed phases |
| 735.00 | 399.37 | 81.56 | 1 bulk, 1 adsorbed phases |
| 750.00 | 405.21 | 85.68 | 1 bulk, 1 adsorbed phases |
| 780.00 | 417.28 | 95.09 | 1 bulk, 1 adsorbed phases |

# 5. CONCLUSION AND FUTURE WORK

## 5.1 Conclusions

In conclusion, this study provided a framework to understand the phase behavior in the bulk phase (inter-particle) and the confined phase (intra-particle). Multiphase equilibrium calculations for fluids confined in the catalyst pores in FTS have been conducted. The PR-C Equation of state model extended to confined fluid has been utilized in multiphase equilibrium algorithm developed by Travalloni et al. [11] using FORTRAN. The simulation results provide the composition and the condition of each bulk phase and pore phase for a given initial mixture. Two different scenarios were investigated: the first one is conventional FTS gas phase at 20 bar and 513 K while the second scenario is supercritical phase at 80 bar and 513 K. The effect of the supercritical solvent hexane is investigated and compared to similar gas phase conditions in which hexane is replaced by nitrogen.

Preferential adsorption of hydrogen has been observed and this could be due to the small size of the hydrogen molecules compared to those of the other components. The results suggest that the supercritical phase provides superior heat dissipation due to the existence of denser phase in the bulk and the confined regions which is in line with experimental observation by Fan et al.[29]. On the other hand, in the gas phase and for limited carbon number (up to $C_8$), the pore phase is found to be in a vapor state which provides higher diffusivity of the reactant than that in the supercritical phase.

44

**5.2 Future Work**

The work presented in this thesis is part of a research project conducted at Texas A&M University at Qatar. The ultimate goal of this research work is to develop novel design for Fischer Tropsch technology via experimental and modeling activities. The modeling part is based on development of a generic program that captures phase behavior of typical FTS reaction mixture in a fixed bed reactor both in the bulk phase (inter-particle) and in the confined catalyst pores (intra-particle). Optimizing the FTS reactor bed performance starts with better understanding of the reaction behavior under typical operating which requires detailed knowledge about the reaction kinetic, better quantification of mass and heat transfer limitations inside the reactor bed and catalyst pores, and quantitative assessment of the role of reaction media on the reaction performance (e.g., supercritical fluids FTS). In general, both qualitative and quantitative knowledge of the aforementioned mentioned phenomena are essential for scaling up new generations of FTS fixed bed reactors. Additionally, in the current study the representation of the hydrocarbons considered only ($C_1$ to $C_8$) while in reality the cobalt catalyst produces much higher carbon number range. The existence of higher hydrocarbons even in small fraction may result in different phenomena such as capillary condensation. It is recommended to incorporate higher carbon numbers in the developed in this study. It is also recommended to investigate the effect of temperature change on the phase behavior as in our study we fixed the temperature.

This thesis represents a preliminary study that will be incorporated in the overall FTS simulation model. The EOS for confined fluids model will be linked to the kinetic model that exists for FTS in fixed bed reactors. The expectation is to calculate more accurate concentration profiles along the reactor by taking into account the confined phase behavior. Experimental data could be used to validate and further improve the model. The finding of this study and the developed models could be verified using the advanced bench-scale fixed-bed reactor currently in operation at Texas A&M University Qatar. More importantly, the visualization of the reactor *in-situ* behavior, which will be conducted utilizing advanced MRI and NMR facilities at the University of Cambridge, could as well provide accurate measurements of diffusivities and other transport properties.

## REFERENCES

1.  Van Der Waals, J.D. and J.S. Rowlinson, *On the Continuity of the Gaseous and Liquid States* 2004: Dover Publications.

2.  Peng, D.-Y. and D.B. Robinson, *A New Two-Constant Equation of State.* Industrial & Engineering Chemistry Fundamentals, 1976. **15**(1): p. 59-64.

3.  Soave, G., *Equilibrium Constants from a Modified Redlich-Kwong Equation of State.* Chemical Engineering Science, 1972. **27**(6): p. 1197-1203.

4.  Patel, N.C. and A.S. Teja, *A New Cubic Equation of State for Fluids and Fluid Mixtures.* Chemical Engineering Science, 1982. **37**(3): p. 463-473.

5.  Goodwin, A.R.H., J.V. Sengers, C.J. Peters, R.S.o. Chemistry, I.U.o. Pure, A.C. Physical, B.C. Division, and I.A.o.C. Thermodynamics, *Applied Thermodynamics of Fluids* 2010: Royal Society of Chemistry.

6.  Chen, C.-C. and P.M. Mathias, *Applied Thermodynamics for Process Modeling.* American Institute of Chemical Engineers. AIChE Journal, 2002. **48**(2): p. 194.

7.  Tsonopoulos, C. and J.M. Prausnitz, *A Review for Engineering Applications.* Cryogenics, 1969. **9**(5): p. 315-327.

8.  Valderrama, J.O., *The State of the Cubic Equations of State.* Industrial & Engineering Chemistry Research, 2003. **42**(8): p. 1603-1618.

9.  Martin, J.J., *Cubic Equations of State-Which?.* Industrial & Engineering Chemistry Fundamentals, 1979. **18**(2): p. 81-97.

10. Frenkel, D. and B. Smit, *Understanding Molecular Simulation: From Algorithms to Applications.* 2001: Elsevier Science.

11. Travalloni, L., M. Castier, and F.W. Tavares, *Phase Equilibrium of Fluids Confined in Porous Media from an Extended Peng–Robinson Equation of State.* Fluid Phase Equilibria, 2014. **362**(0): p. 335-341.

12. Travalloni, L., M. Castier, F.W. Tavares, and S.I. Sandler, *Thermodynamic Modeling of Confined Fluids Using an Extension of the Generalized van der Waals Theory.* Chemical Engineering Science, 2010. **65**(10): p. 3088-3099.

13. Travalloni, L., M. Castier, F.W. Tavares, and S.I. Sandler, *Critical Behavior of Pure Confined Fluids from an Extension of the van der Waals Equation of State.* The Journal of Supercritical Fluids, 2010. **55**(2): p. 455-461.

14. Sandler, S.I., *From Molecular Theory to Thermodynamic Models.* Chemical Engineering Education, 1990. **24**(1): p. 12-19.

15. Spath, Pamela L., Dayton D. C. *Preliminary Screening--Technical and Economic Assessment of Synthesis Gas to Fuels and Chemicals with Emphasis on the Potential for Biomass-derived Syngas*. 2003; Available from: http://purl.access.gpo.gov/GPO/LPS47916.

16. Elbashir, N.O. and C.B. Roberts, *Enhanced Incorporation of α-Olefins in the Fischer−Tropsch Synthesis Chain-Growth Process over an Alumina-Supported Cobalt Catalyst in Near-Critical and Supercritical Hexane Media.* Industrial & Engineering Chemistry Research, 2005. **44**(3): p. 505-521.

17. Schulz, H., *Short History and Present Trends of Fischer–Tropsch Synthesis.* Applied Catalysis A: General, 1999. **186**(1–2): p. 3-12.

18.     Chedid, R., M. Kobrosly, and R. Ghajar, *The Potential of Gas-to-Liquid Technology in the Energy Market: The Case of Qatar.* Energy Policy, 2007. **35**(10): p. 4799-4811.

19.     Yokota, K. and K. Fujimoto, *Supercritical-Phase Fischer-Tropsch Synthesis Reaction. 2. The Effective Diffusion of Reactant and Products in the Supercritical-Phase Reaction.* Industrial & Engineering Chemistry Research, 1991. **30**(1): p. 95-100.

20.     Huang, X., C.W. Curtis, and C.B. Roberts, *Reaction Behavior of Fischer-Tropsch Synthesis in Near Critical and Supercritical Hexane Media*, 2002. p. 150-153.

21.     Lee, T.S. and J.N. Chung, *Mathematical Modeling and Numerical Simulation of a Fischer–Tropsch Packed Bed Reactor and Its Thermal Management for Liquid Hydrocarbon Fuel Production using Biomass Syngas.* Energy & Fuels, 2012. **26**(2): p. 1363-1379.

22.     Ermolaev, V.S., V.Z. Mordkovich, and I.G. Solomonik, *Influence of Capillary Condensation on Heat and Mass Transfer in the Grain of a Fischer-Tropsch Synthesis Catalyst.* Theoretical Foundations of Chemical Engineering, 2010. **44**(5): p. 660-664.

23.     Mogalicherla, A.K., E.E. Elmalik, and N.O. Elbashir, *Enhancement in the Intraparticle Diffusion in the Supercritical Phase Fischer–Tropsch Synthesis.* Chemical Engineering and Processing: Process Intensification, 2012. **62**(0): p. 59-68.

24. Sandler, S.I., *An Introduction to Applied Statistical Thermodynamics.* 2011, Hoboken, NJ: Hoboken, NJ : Wiley.

25. Castier, M. and M.M. Amer, *XSEOS: An Evolving Tool for Teaching Chemical Engineering Thermodynamics.* Education for Chemical Engineers, 2011. **6**(2): p. e62-e70.

26. Cabral, V.F., M. Castier, and F.W. Tavares, *Thermodynamic Equilibrium in Systems with Multiple Adsorbed and Bulk Phases.* Chemical Engineering Science, 2005. **60**(6): p. 1773-1782.

27. Morris, A.J., *Numerical Methods for Unconstrained Optimization, Ed. W. Murray, Academic Press, London.* International Journal for Numerical Methods in Engineering, 1973. **6**(4): p. 608-608.

28. Elmalik, E.E., E. Tora, M. El-Halwagi, and N.O. Elbashir, *Solvent Selection for Commercial Supercritical Fischer–Tropsch Synthesis Process.* Fuel Processing Technology, 2011. **92**(8): p. 1525-1530.

29. Fan, L. and K. Fujimoto, *Fischer–Tropsch Synthesis in Supercritical Fluid: Characteristics and Application.* Applied Catalysis A: General, 1999. **186**(1–2): p. 343-354.

30. Kim, D.J., J.E. Yie, and S.G. Seo, *Adsorption Isotherms of CO and VOCs on Hydrocarbon Adsorbers of Honeycomb Shape.* Journal of Chemical & Engineering Data, 2003. **48**(6): p. 1471-1475.

31. Nam, G.-M., B.-M. Jeong, S.-H. Kang, B.-K. Lee, and D.-K. Choi, *Equilibrium Isotherms of CH4, C2H6, C2H4, N2, and H2 on Zeolite 5A Using a Static*

*Volumetric Method.* Journal of Chemical & Engineering Data, 2004. **50**(1): p. 72-76.

32. Kim, J.-H., C.-H. Lee, W.-S. Kim, J.-S. Lee, J.-T. Kim, J.-K. Suh, and J.-M. Lee, *Adsorption Equilibria of Water Vapor on Alumina, Zeolite 13X, and a Zeolite X/Activated Carbon Composite.* Journal of Chemical & Engineering Data, 2002. **48**(1): p. 137-141.

33. Danner, R.P. and L.A. Wenzel, *Adsorption of Carbon Monoxide-Nitrogen, Carbon Monoxide-Oxygen, and Oxygen-Nitrogen Mixtures on Synthetic Zeolites.* AIChE Journal, 1969. **15**(4): p. 515-520.

34. Lee, J.-W., H.-C. Kang, W.-G. Shim, C. Kim, and H. Moon, *Methane Adsorption on Multi-Walled Carbon Nanotube at (303.15, 313.15, and 323.15) K.* Journal of Chemical & Engineering Data, 2006. **51**(3): p. 963-967.

35. McMinn, J.T.D., PhD Thesis, University of Texas, 1952.

**APPENDIX A**

**Parameters Fitting**

The characteristic size parameter $\delta_{p,i}$ and characteristic energy parameter $\varepsilon_{p,i}$ for the model has been estimated by fitting adsorption experimental data using XSEOS thermodynamic computational package for Excel ® as described in section 3.3.

### A.1 Carbon Monoxide Parameters

Carbon monoxide parameters were estimated by fitting experimental adsorption data [30] on Activated alumina as shown in Figure 12. The size parameter was found to be equal to ($\delta_p/\sigma_p = 0.5250$) while the energy parameter to be equal to ($\varepsilon_p/k = 1390.815$).
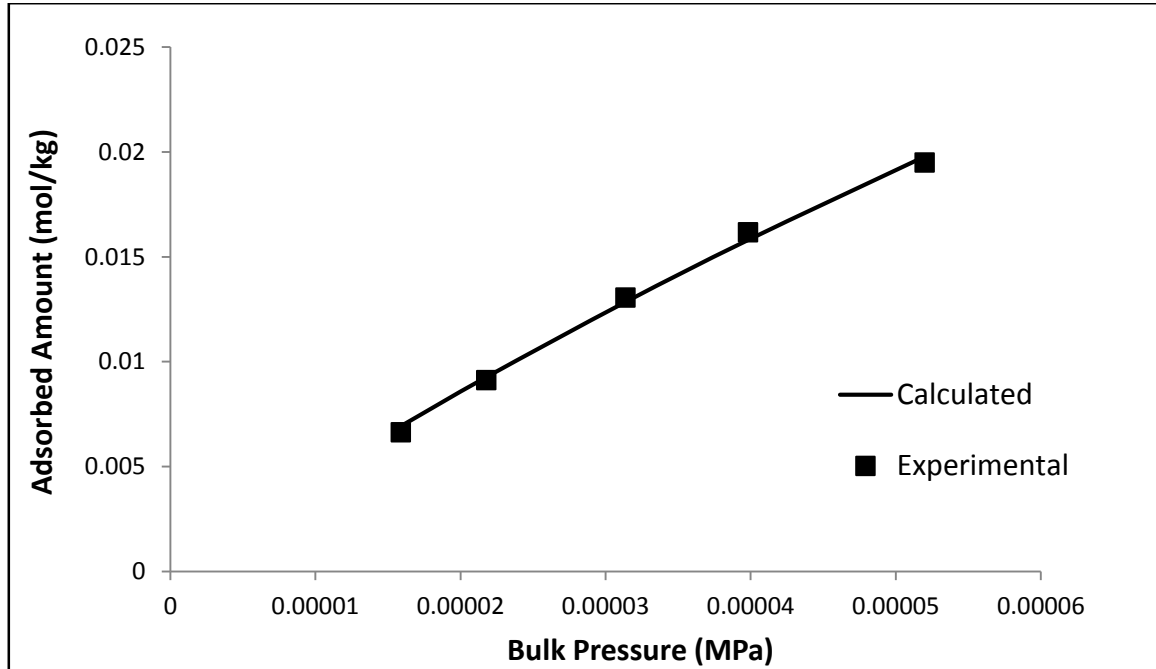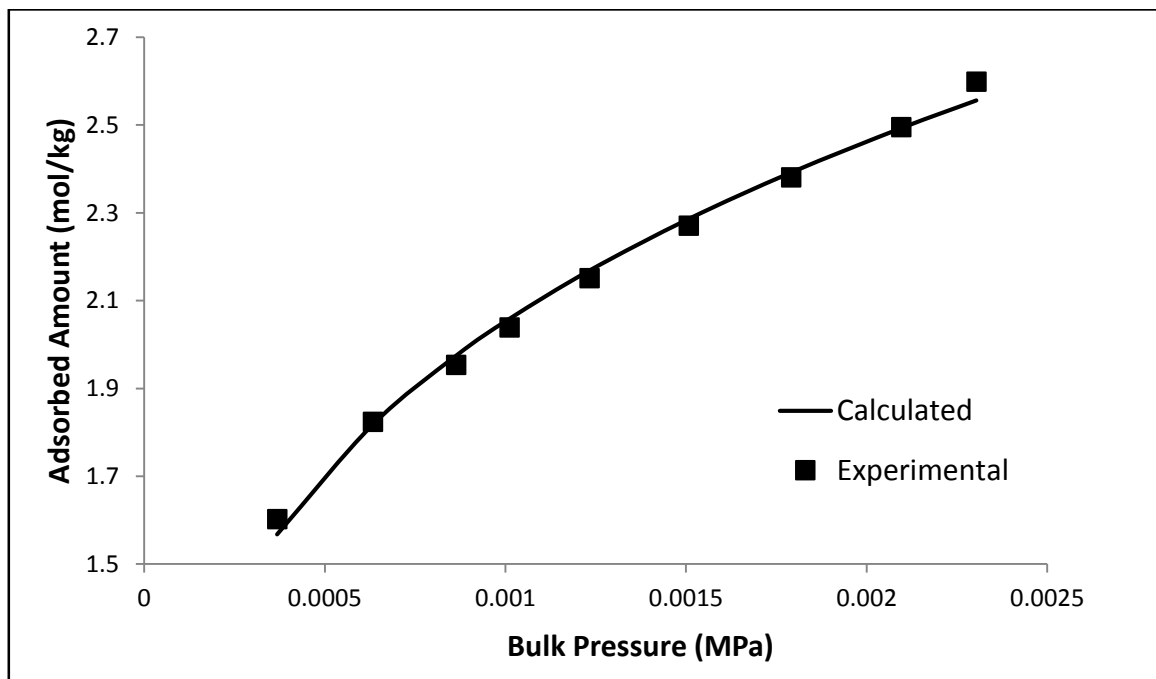


**Figure 12 :** Parameter estimation for carbon monoxide on activated alumina at 303.15 K

## A.2 Hydrogen Parameters

Hydrogen parameters were estimated by fitting experimental adsorption data[31] on zeolite A due to the lack of data for adsorption on Activated alumina as shown in Figure 13. The size parameter was found to be equal to ($\delta_p/\sigma_p = 1.231$) while the energy parameter to be equal to ($\varepsilon_p/k = -2119.772$).
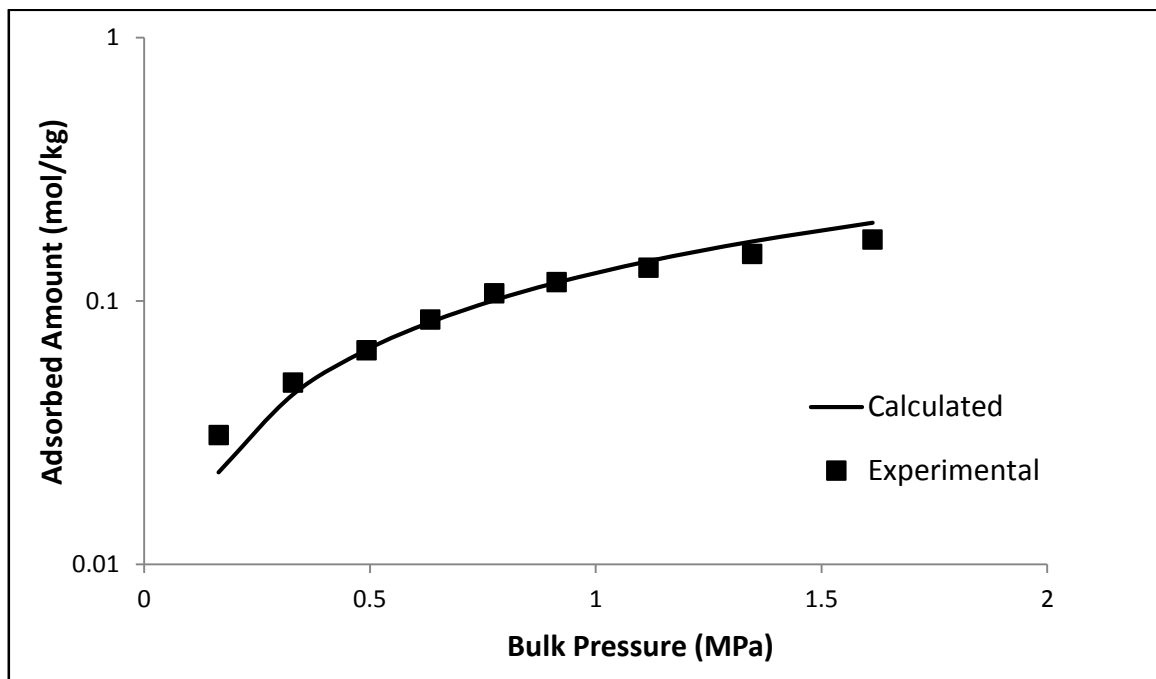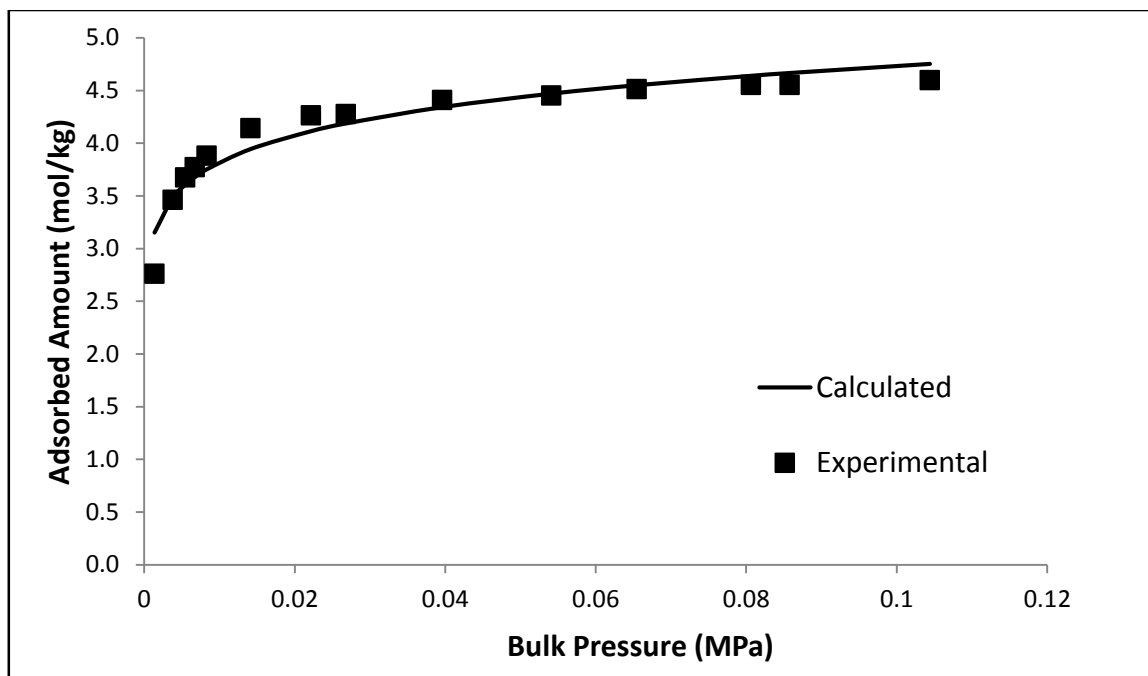


**Figure 13 :** Parameter estimation for hydrogen on zeolite A at 313.15 K

## A.3 Water Parameters

Water parameters were estimated by fitting experimental adsorption data [32] on Activated alumina as shown in Figure 14. The size parameter was found to be equal to ($\delta_p/\sigma_p = 0.9814$) while the energy parameter to be equal to ($\varepsilon_p/k = 5082.668$).
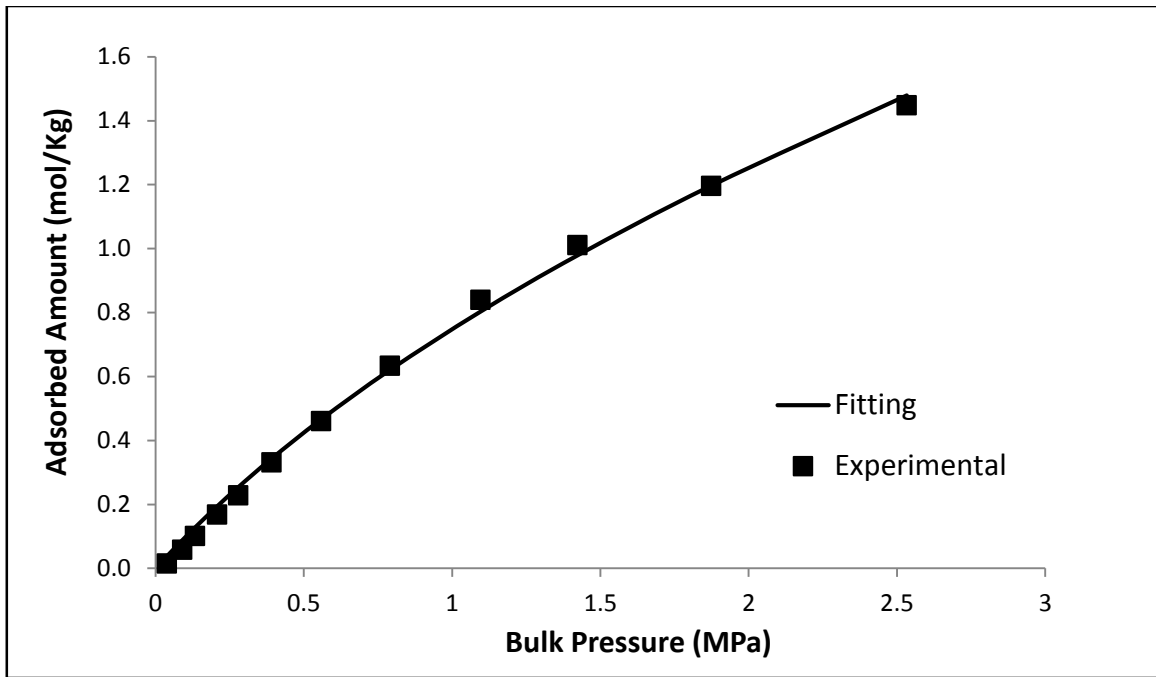


**Figure 14 :** Parameter estimation for water on activated alumina at 353.15 K

## A.4 Nitrogen Parameters

Nitrogen were estimated by fitting experimental adsorption data [33] on zeolite A due to the lack of data for adsorption on Activated alumina as shown in Figure 15. The

size parameter was found to be equal to ($\delta_p/\sigma_p = 0.1211$) while the energy parameter to be

equal to ($\varepsilon_p/k = 3112.913$).



**Figure 15 :** Parameter estimation for nitrogen on zeolite A at 144.261 K

### A.5 Methane Parameters (C₁)

Methane parameters were estimated by fitting experimental adsorption data [34]

on Activated alumina as shown in Figure 16. The size parameter was found to be equal to

($\delta_p/\sigma_p = 0.8804$) while the energy parameter to be equal to ($\varepsilon_p/k = 798.024$).

**Figure 16 :** Parameter estimation for methane on activated alumina at 323.15 K

### A.6 Ethane Parameters (C$_2$)

Ethane parameters were estimated by fitting experimental adsorption data [35] on Activated alumina as shown in Figure 17. The size parameter was found to be equal to ($\delta_p/\sigma_p = 0.7980$) while the energy parameter to be equal to ($\varepsilon_p/k = 1026.135$).
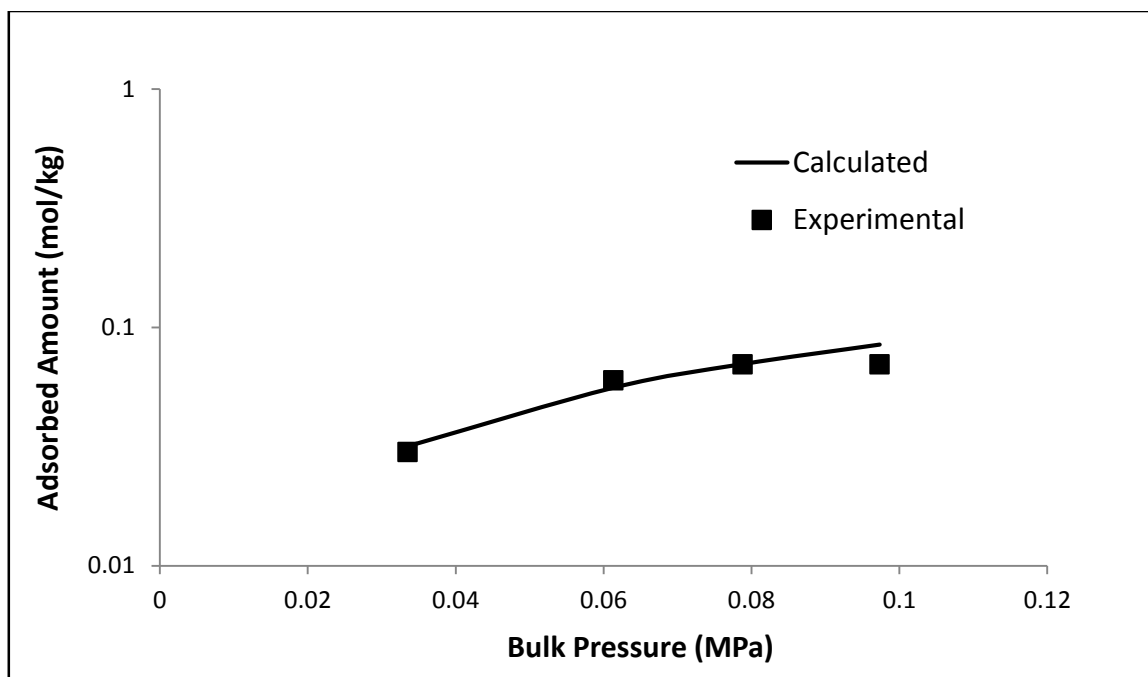
**Figure 17 :** Parameter estimation for ethane on activated alumina at 313.15 K

## A.7 Propane Parameters (C₃)

Propane parameters were estimated by fitting experimental adsorption data [35] on Activated alumina as shown in Figure 18. The size parameter was found to be equal to ($\delta_p/\sigma_p = 0.7156$) while the energy parameter to be equal to ($\varepsilon_p/k = 1254.245$).
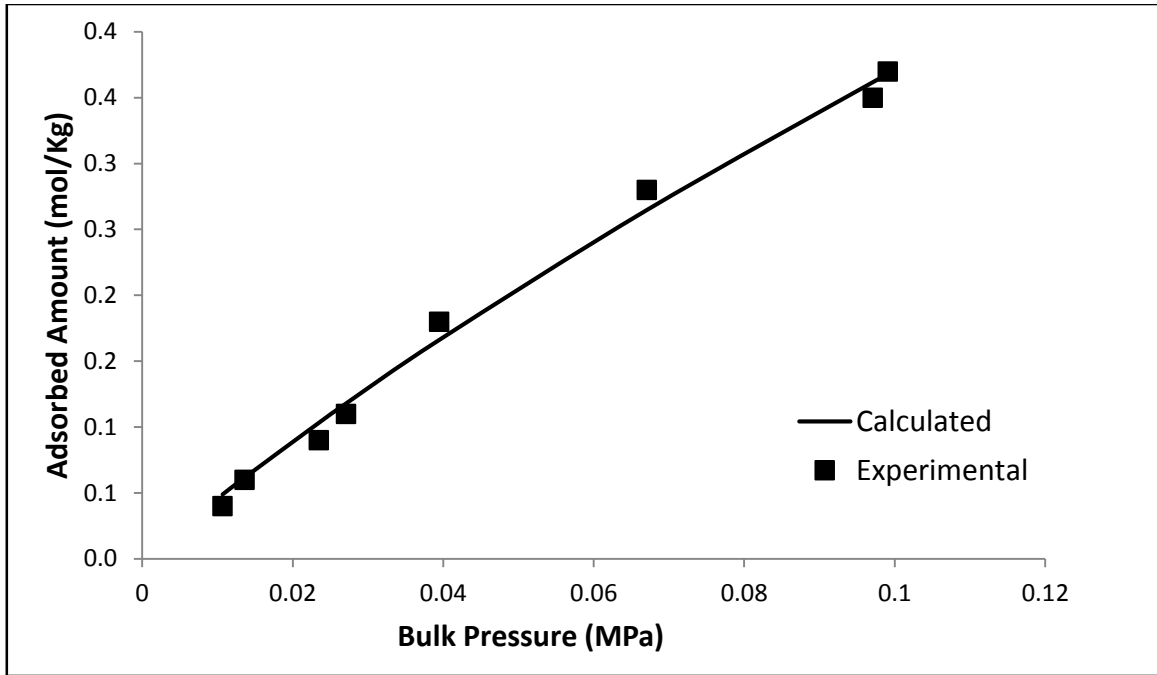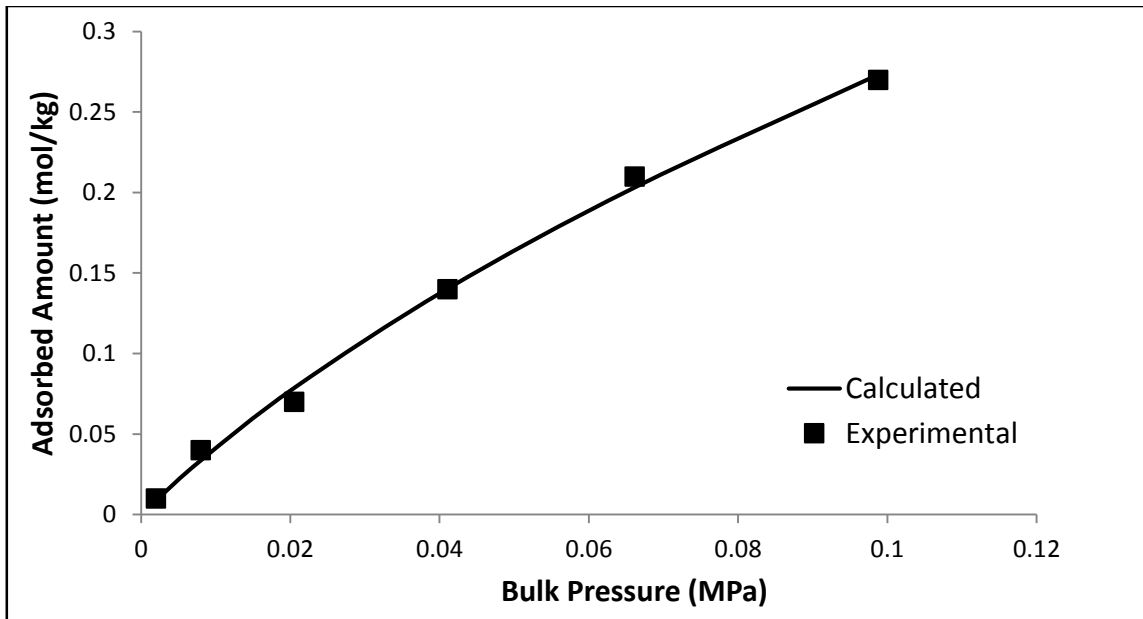
**Figure 18 :** Parameter estimation for propane on activated alumina at 313.15 K

## A.8 Butane Parameters (C$_4$)

Butane parameters were estimated by fitting experimental adsorption data [35] on Activated alumina as shown in Figure 19. The size parameter was found to be equal to ($\delta_p/\sigma_p$ = 0.3481) while the energy parameter to be equal to ($\varepsilon_p/k$ = 1279.653).

**Figure 19 :** Parameter estimation for butane on activated Alumina at 313.15 K

### A.9 2,2-Dimethyl propane Parameters (C$_5$)

2,2-Dimethyl propane parameters were estimated by fitting experimental adsorption data [35] on Activated alumina as shown in Figure 20. The size parameter was found to be equal to ($\delta_p/\sigma_p = 0.1779$) while the energy parameter to be equal to ($\varepsilon_p/k = 1797.517$).
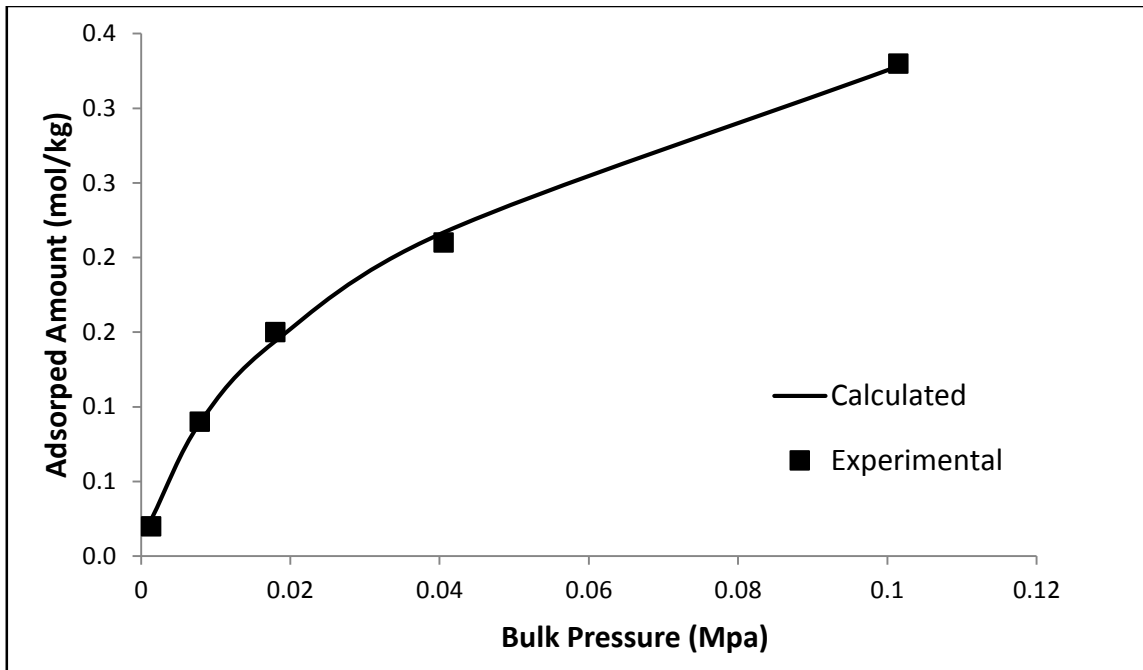
**Figure 20 :** Parameter estimation for 2-methyl propane on activated alumina at 313.15 K

### A.10 2,2,4-Trimethyl pentane Parameters (C$_8$)

2,2,4-Trimethyl pentane parameters were estimated by fitting experimental adsorption data [30] on Activated alumina as shown in Figure 21. The size parameter was found to be equal to ($\delta_p/\sigma_p = 0.1117$) while the energy parameter to be equal to ($\varepsilon_p/k = 2817.953$).
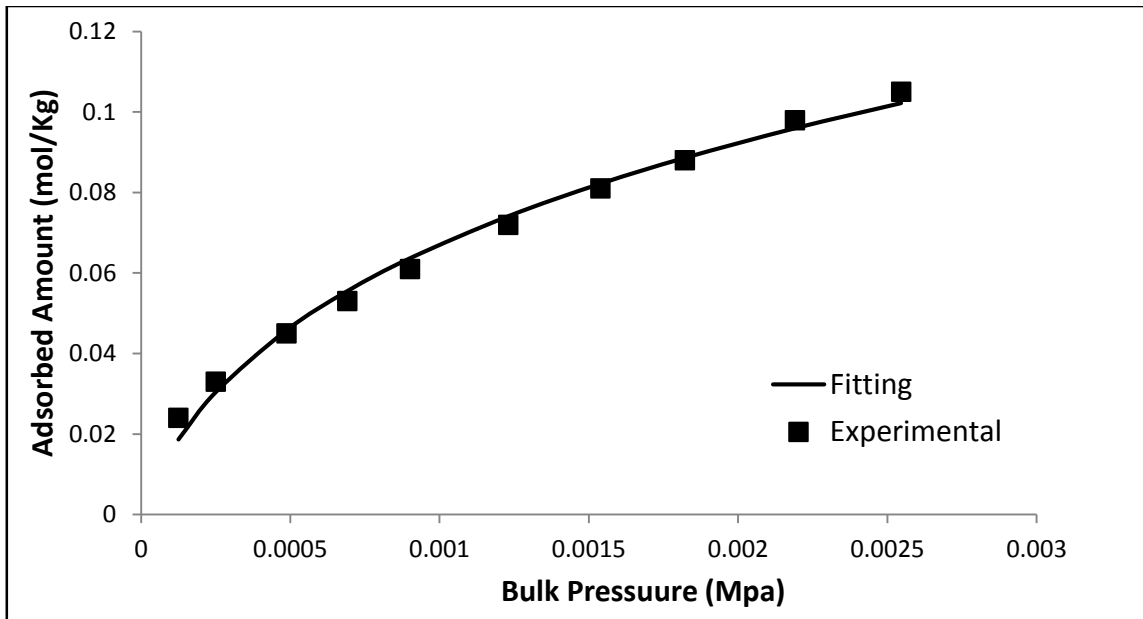
**Figure 21 :** Parameter estimation for 2,2,4-trimethyl pentane on activated alumina at 343.15 K